RADAR-BASED HEARTBEAT ESTIMATION FOR INDOOR HEALTHCARE APPLICATIONS

MASTER THESIS REPORT

Author:
Huixuan Chen (5409705)

August 23, 2023

This thesis has been approved by
Responsible Professor: dr. F. Fioranelli

Thesis committee:
Dr. F. Fioranelli, EWI-ME-MS3, Delft University of Technology
Dr. B. Hunyadi, EWI-ME-SPS, Delft University of Technology

ACKNOWLEDGMENTS

Time flies, two years have passed. The time spent in TU Delft is a precious memory for me. It is time for the end of the graduation thesis, I can not do it without the help of everyone around me looking back on nine months.

Firstly, I would like to express great gratitude to my thesis supervisor, Prof.Francesco Fioranelli. Thank you for providing me the chance to work on this project about health-care which I am interested in, enjoyable, and want to continue in my career. In the weekly meeting, he always gives me valuable feedback to guide my work on the right road. In my medium-term presentation, I'm very grateful for the detailed notes he gave me. I really appreciate the support and help which give me the confidence to overcome the difficulties during the thesis project.

Secondly, I sincerely appreciate all the professors, Ph.D. students, researchers, and Master's students in Microwave Sensing, Signals, and Systems Group. Thank you for sharing in the seminar every week, I learn a lot not only the knowledge but you're your passion for academic research. I also want to thank Dr. JianpingWang for the discussion and advice for my project, Ph.D. student Ronny Guendel, Sen Yuan, and MSc student Max Cortés Peralta for helping with the radar setup and measurement. Test volunteer Dr. Dingyang Wang, Master students Xiangwen Wang, Wenyi Lu, Fan Lei, Wenxu Chen, Jialin Lyu, and Jiaxuan Xiao, thank you for providing the experiment data.

Then, I also want to thank my family and friends. The process of studying at TU Delft is not always smooth, sometimes full of pressure and difficulties, thank you for always accompanying me to encourage me to face the difficulties!

ABSTRACT

With the aging population, the demand for healthcare and related services is increasing and, for this reason, technologies for remote patient monitoring are developing, aiming at indoor scenarios. Remote patient monitoring can help capture the clinical data of patients at home, which can save time and money, specifically reducing the need for hospitalization by potentially detecting health-related issues before they become too serious.

The non-contact radar-based technology can be applied in the remote patient monitoring system for detecting vital signs. Radars are suitable for applications at home because they are non-invasive, robust in changing lighting and temperature, and suitable for patients with skin irritation.

Heartbeat and respiration are critical clinical data for the diagnosis of the disease. The study of respiration frequency estimation was explored by previous work, such as the MSc thesis in [1]. Building on that work, this project proposes a pipeline to measure the heartbeat frequency and cancel the random body movement. The impact of different orientations is also studied. The phase history difference of the chest displacement due to vital signs is extracted, and the wavelet transform is used to separate heartbeat and respiration signals. Different methods are tested to calculate the heartbeat frequency in the time and frequency domain. The RBM is detected by the energy threshold of the phase difference, and the intervals with the RBM are discarded.

The simulation and experimental results indicate that the proposed processing pipeline can work on the radar data.

CONTENTS

ABBREVIATIONS

AC auto-correlation-based movement detection method. 9

AKF adaptive Kalman filter. 9

AR auto-regressive algorithm. 12

ARA advanced range-bin alignment technique. 9

CF curve fitting technology. 9

ECG electrocardiogram. 1

EKF extended Kalman filter. 12

EMD empirical mode decomposition. 11

FIR finite impulse response filter. 11

FMCW Frequency modulated continuous wave. 2, 11

GT Gabor transform. 11

ICA independent component analysis. 10

IMF intrinsic mode functions. 11

IR-UWB impulse radio ultra-wideband. 10

KF Kalman filter. 12

KFT Kalman filter-based tracking algorithm. 12

MDM multi-direction measurement method. 9

MSM multi-sensor measurement. 9

MTI moving target indicator. 10

PCC principal component combining. 12

RBM random body movement. 9

RCS radar cross section. 40, 46, 49

RPM remote patient monitoring. 1

RPS remote patient system. 1

VMD variational mode decomposition. 11

WICA wavelet independent component analysis. 10

WT wavelet transform. 11

List of Figures

List of Tables

1

INTRODUCTION

In this introduction chapter, the background, the problem statement and contribution, and the outline are described. The background in Section 1.1 shows why the thesis is conducted. The statement about the problems the thesis project addresses is analyzed in Section 1.2. In Section 1.3, the expected contributions at the end of the project are shown. In Section 1.4, the outline of the report is presented.

1.1. BACKGROUND

As people's requirements for healthcare become higher and medical resources in hospitals are limited, remote patient monitoring (RPM) is constantly developing to provide the service to monitor patients at home. Some devices such as wearable electrocardiogram (ECG) monitors, smart health watches, radars, and biosensors capture clinical data such as heartbeat, blood pressure, and respiration rate. These data can be shared with healthcare professionals such as healthcare monitoring centers, hospitals, and skilled nursing facilities for consultation, emergency warnings, and chronic conditions treatments [2]. RPM systems can help save time and money for patients and manage limited medical resources more effectively.

Heartbeat and respiration are critical vital signs for the disease diagnosis of the human body. Heartbeat rate may be an essential risk factor for sudden coronary heart disease (CHD) death and related to the causes of mortality [3]. The combined effect of heart rate and other cardiovascular diseases can lead to death from cardiovascular diseases (CVD) and non-sudden CHD [3]. The resting heartbeat rate is a clinical parameter that not only plays one of the fundamental roles in emergency patients, but is also helpful in preventing chronic diseases in healthy subjects [4]. It can be used to predict coronary artery disease, stroke, sudden death, and non-cardiovascular diseases independently [5].

Contact devices for measuring vital signs in remote patient system (RPS) to measure heartbeat, such as wearable ECG monitors and smart health watches, may lead to allergic reactions, skin irritation, limit movement, and comfort of users [6]. Wearable ECG monitors like the chest strap measuring the electrical activity of your heartbeat

have higher accuracy than smart health watches using sensors that measure heartbeats based on blood vessels [6]. But smartwatches are more comfortable than the chest strap because of less area of friction with clothing and skin. Wet and dry electrodes are also common biosensors that need to be in contact with the skin, which may have lower accuracy because of the unstable contact [7].

In addition to the accuracy of the heartbeat measurement, the lightweight and comfort are essential in indoor healthcare [7]. So non-contact techniques can be better choices to improve the user experience. Non-contact technologies like laser Doppler vibrometry (LDV), airborne ultrasound, cameras, and radio frequency (RF) technology can be used to detect vital signs [7]. LDV measures heartbeat and respiration rates by displacement of the chest skin, but its size and complexity make it hard to be widely used [8]. Airborne ultrasound can accurately estimate the heartbeat rate for people with clothes, but the system is cumbersome [9]. Both of them have a high price to be applied in indoor healthcare. RF technology like passive RFID tags has a low cost to monitor the heartbeat and breathing based on chest movement, but it is harder to detect weak heartbeat precisely and needs to attach tags on the clothes [10]. Another RF-based technology, radar systems, is also suitable for home applications because they are non-invasive compared with cameras, robust to changing lighting and temperature, and can detect vital signs even for sleeping people or babies without sticky on-body sensors [11]. Frequency modulated continuous wave (FMCW) radar is a type of radar that is capable of measuring the range and velocity via Doppler frequency, and it is widely applied in indoor vital sign measurement [12].

Based on the requirement for indoor healthcare and the discussion of technologies, the focus of this thesis is on monitoring vital signs via FMCW radar.

1.2. PROBLEM STATEMENT

This thesis project follows up on the MSc thesis by Irving Maximino Cortés Peralta, a former MSc student of the MS3 group [1]. His project involved joint human motion recognition and breathing frequency estimation for indoor healthcare applications based on FMCW radar [1]. In-place (sitting) and translational (walking and standing) activities are separated first, then the extended Kalman Filter (EKF) estimated the breathing frequency during the in-place scenario. This project has three main goals: extending current monitoring capabilities to heartbeat, analyzing the impact of different orientations of the targets, and canceling random body movement (RBM). Some challenges are listed as follows:

The extension of current capabilities to heartbeat

The previous work in [1] focused on respiration estimation, the heartbeat was out of scope. However, the heartbeat is also an important clinical parameter worth extending the current capabilities. There are some challenges for radar-based heartbeat frequency estimation.

- The heartbeat signal is weaker than the respiration signal. The waveform and algorithm's design must be capable of detecting heartbeat signals. The data with heartbeat information needs to be selected.

- The possible frequency band of the heartbeat needs to be researched. The heartbeat and respiration activities have a low and close frequency, so accurate separation and estimation of two vital signs need to be researched.
- The performance of the algorithm needs to be verified to be robust enough to possible heartbeat frequencies by the simulations and experiments. The experiment scenario needs to be designed.

The cancellation of random body movement (RBM)
Random body movement (RBM) may occur during the measurement at any time. The user experience of the patient at home is influenced by the limitation of body movement. The achievement of RBM cancellation can also improve the accuracy of vital sign estimation, especially for the weak heartbeat signal. The tasks for the RBM cancellation are described below.

- In this project, the large-scale RBM like shaking hands and large chest movement that is much larger than the movement due to the vital signs, needs to be detected and canceled.
- A model of RBM needs to be researched and implemented in the simulation used to test the algorithm's performance.
- In the experiments, the RBM is defined as random movements larger than chest displacement due to the vital sign. The accuracy of RBM cancellation should be analyzed.

Analysis of the impact of different orientations of the targets
The targets sat on a chair and faced the radar to measure the respiration signal in [1]. Whether the orientation of the targets will influence the accuracy of the estimation and whether the front side is the optimal measurement direction is not studied in previous work in [1]. The study of the different orientations can provide the possibility of increasing the activity space for a better user experience. The different orientations should be selected and tested, and the performance should be evaluated in this project.

1.3. THESIS CONTRIBUTION

The main contributions of this thesis are summarized below:

(1) A processing pipeline with an explanation of the methods for extracting and estimating the heartbeat from the radar signal is proposed.

(2) The algorithm used to accurately estimate the heartbeat signal is implemented in MATLAB.

(3) The waveform that can be used to extract heartbeat activity from FMCW radar is designed and validated.

(4) The proposed pipeline is validated with simulated and experimental radar data of 7 participants. Random body movement can be canceled, and the impact of the body orientation is studied.

1

1.4. THESIS OUTLINE

The rest of the thesis is structured as follows. Chapter 2 reviews the most relevant literature on heartbeat estimation, the impact of different body orientations, and RBM cancellation. Chapter 3 selects and assembles the different ideas from the literature into a complete process pipeline. The design of the chosen radar waveform is also described. Chapter 4 presents the simulations in MATLAB and the analysis of the results. The measurement equipment, experiment design, and analysis of the experimental results are introduced in Chapter 5. Finally, the conclusions and recommendations are presented in Chapter 6.

2

LITERATURE REVIEW

This chapter reviews the most relevant literature on vital sign monitoring by radars. Section 2.1 introduces the cardiopulmonary activity and the model of vital signs and radar data. Section 2.2 describes the existing signal processing approaches to remove clutter, random body movement cancellation, and estimation of the heartbeat frequency. In the end, the literature review is summarized in Section 2.3.

2.1. SIGNAL MODEL

2.1.1. PHYSIOLOGY OF CARDIOPULMONARY ACTIVITY

The FMCW radar can measure chest displacement to extract information on vital signs. The chest displacement due to vital signs is very small and can not be detected with the range resolution of the FMCW radar. The phase history in slow time contains the vital sign information and can be converted to range history [13]. The Doppler resolution of the FMCW radar can detect the low frequency of vital signs. The detailed calculation is explained in 2.1.2. The process from the beginning of the heartbeat to the beginning of the next heartbeat is the cardiac cycle [14]. The cardiac cycle has two periods, which are diastole and systole [14]. In the diastole period, the heart relaxes, filled with blood in the systole. The electrocardiogram is shown in Figure 2.1. The voltages of the heart are recorded from the surface of the body [14]. The ventricular volume resulting in the chest surface displacement can be extracted by radar to further vital sign estimation. The heartbeat causes the chest displacements between 0.3 and 0.8 mm [15]. The heartbeat rate (HR) corresponds to a frequency between 1 and 3 Hz.

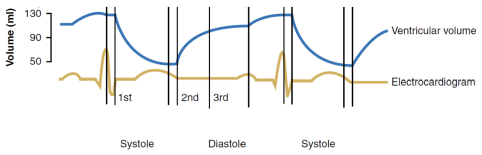

Figure 2.1: Ventricular volume changes and electrocardiogram during heartbeat [14]

In the process of respiration, oxygen is provided to the body, and carbon dioxide leaves. There are two activities in respiration duration shown in Figure 2.2. During inspiration(left side), the diaphragm contracts, pulling the lower surfaces of the lungs down. During expiration(right side), the diaphragm relaxes, and the lungs are compressed to remove the air. The changes in lung volume, which will result in the displacement of the chest surface are shown in Figure 2.3. The chest displacement due to the respiration activity between 3 mm and 11 mm [16]. The respiration rate (RR) varies between 0.1 and 0.3 Hz [17].

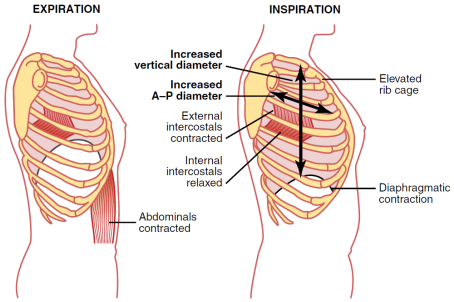

Figure 2.2: Contraction and expansion of the thoracic cage during expiration and inspiration [14]

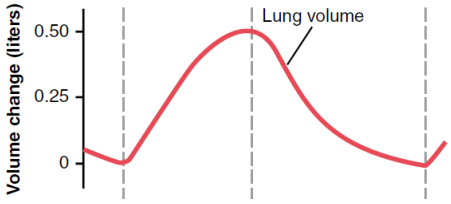

Figure 2.3: The changes in lung volume during respiration cycle [14]

2.1.2. VITAL SIGN MODEL

In many studies, the human chest surface caused by breathing and heartbeat are considered as periodic motions with different amplitudes and frequencies [18]. The derivations of models are proposed by Paterniani et al. [19].

The movement of the chest surface due to heartbeat can be modeled as the displacement in Equation 2.1.

$$R_h(t) \approx \alpha_h cos(2\pi f_h t) \tag{2.1}$$

where α_h is deterministic, unknown amplitude, f_h is deterministic, unknown angular frequency and φ_h is initial phase of the heartbeat signal.
Similarly, the movement of the chest surface due to respiration can also be modeled as a

displacement in Equation 2.2.

$$R_r(t) \approx \frac{\alpha_r\,(1-cos(2\pi f_r t))}{2} \tag{2.2}$$

where α_r is deterministic and unknown amplitude, f_r is deterministic and unknown angular frequency and φ_r is initial phase of the respiration signal.
For simplicity here, respiration and heartbeat are separated because studying their interaction goes beyond the scope of this thesis. The total displacement of the chest surface can be expressed by the summation of two movements in Equation 2.3.

$$\begin{aligned} R(t) &= R_h(t) + R_r(t) \\ &= \frac{\alpha_r\,(1-cos(2\pi f_r t))}{2} + \alpha_h cos(2\pi f_h t) \end{aligned} \tag{2.3}$$

2.1.3. RADAR RESPONSE MODEL OF THE VITAL SIGN

If the initial position of the chest surface is R_0, then the position of the chest surface at a distance R_0 can be expressed by Equation 2.4.

$$\begin{aligned} R(t) &= R_0 + R_r(t) + R_h(t) \\ &= R_0 + \frac{\alpha_r\,(1-cos(2\pi f_r t))}{2} + \alpha_h cos(2\pi f_h t) \end{aligned} \tag{2.4}$$

The phase history $\phi_{ph}(n)$ over slow time is derived by Equation 2.5.

$$\begin{aligned} \phi_{ph}(t) &= \frac{4\pi f_c}{c} R(t) \\ &= \frac{4\pi f_c}{c}\left(\frac{\alpha_r\,(1-cos(2\pi f_r t))}{2} + \alpha_h cos(2\pi f_h t)\right) \end{aligned} \tag{2.5}$$

Because there is an initial distance R_0 between the radar and the chest surface of the target, the wrapped phase caused can be written by Equation 2.6.

$$\phi_e = wrap\left(\frac{4\pi f_c}{c} R_0\right) \tag{2.6}$$

The phase history can be expressed as Equation 2.7.

$$\phi_{ph}(t) = \phi_e + \frac{4\pi f_c}{c}\left(\frac{\alpha_r\,(1-cos(2\pi f_r t))}{2} + \alpha_h cos(2\pi f_h t)\right) \tag{2.7}$$

The range history over slow time can be computed by Equation 2.8 based on the phase history.

$$R(t) = \frac{\phi_{ph}(t)c}{4\pi f_c} \tag{2.8}$$

The beat signal of the range bins in the time domain measured by FMCW radar can be derived in Equation 2.9.

$$s(t) = h\exp(j\phi_e)\exp(j\frac{4\pi f_c}{c}(\frac{\alpha_r\,(1-cos(2\pi f_r t))}{2} + \alpha_h cos(2\pi f_h t)) \tag{2.9}$$

where h is the amplitude of the processed signal, and f_c is the carrier frequency of the radar.

2.2. SIGNAL PROCESSING

The signal processing of the heartbeat has four main blocks illustrated in Figure 2.4. It is a generic processing pipeline from the literature review. After reading raw data from the FMCW radar, the clutter should be removed to detect the range bin with vital signs. The RBM movement should be detected and canceled before the heartbeat estimation. The heartbeat and respiration frequencies need to be analyzed separately.

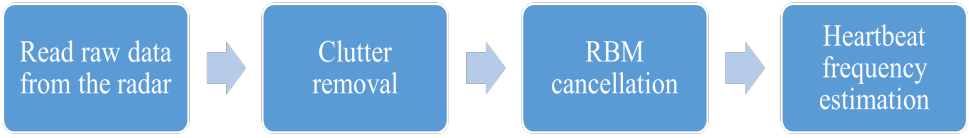

Figure 2.4: A generic processing pipeline from the literature review

2.2.1. CLUTTER REMOVAL

As the heartbeat signal is weak, it can be easily buried by static clutter, which is reflections from the environment. In a static environment, the clutter results in a DC component in the slow-time domain. Lazaro et al. [20] proposed a moving averaging filter that subtracts the average of the received signals to remove the DC component in the fast-time domain. Because the clutter is static, then only the motion of the chest surface varies in slow time. This method provided a good signal-to-noise ratio signal [20]. The window length of the filter should be selected. When the window length is longer, the attenuation of clutter decreases but the cutting-off frequency of the vital sign separation decreases too [20]. An extended method based on this used by Zetik et al. [21] added weighted factors following the exponential law. Sacco et al. [22] used the standard deviation over slow time after the first Fourier transform to reduce the influence of the clutters. Then the signal from the movement of the chest surface can be recognized from the static surroundings. Singh et al. [23] tried to detect respiration behind a wall, and the singular value decomposition (SVD) method was applied to reduce clutter, but it did not work for all kinds of materials. Yim et al. [24] removed unwanted clutter signals by applying the loopback filter for background subtraction.

2.2.2. RANDOM BODY MOVEMENT CANCELLATION

Body movement has a significant influence on the extraction of vital sign signals. Therefore, before applying the process of estimating the heartbeat, the impact of random body movement (RBM) should be reduced. Most papers related to random body movement cancellation did not define the specific motion. It is hard to design further experiments. Khan et al. [25] considered three different types of motions, including speaking, shaking the head slightly, and slight movement of the whole body. The auto-correlation-based movement detection method (AC) determined whether people had random movement based on auto-correlation [25]. The measurement stopped until the people were stationary. This method reduced unreliable measurements, but may lose some information.

Xu et al. [26] built an algorithm based on adaptive Kalman filter (AKF) that updated the model parameters in different activities. This method used the heartbeat and movement history to predict the heartbeat. So the model fitting error may lead to prediction failure. It can work without training data and perform well when the movement changes.

Li et al. [27] used a multi-direction measurement method (MDM), placing two radars in the front and back sides of the people and two synchronized DRSs to detect the RBM. The intense noise was reduced, but the system was complex with multiple radars synchronized.

Gu et al. [28] proposed strategies for RBM cancellation by phase compensation at RF-front-end, baseband, and RBM cancellation for demodulated signals. The multi-sensor measurement (MSM) used the radar system with camera-aided to measure RBM.

Lv et al. [29] applied the curve fitting technology (CF) to compensate for the large-scale body movement. The heartbeat signal was reconstructed from strong body movement noise, but the SNR is low, which needs to be improved.

advanced range-bin alignment technique (ARA) used two incoherent FMCW radars and combined with range history extracted by range-bin alignment method was done by Muñoz-Ferreras [30]. Reflection from the front scatterer is aligned and peaks of the heartbeat and respiration are clear [30].

Adiprabowo et al. [31] used the energy threshold to detect the RBM. If the energy of the heartbeat signal is higher than the threshold, this time segment is removed because there is an RBM here. This method is simple and effective for large-scale movement. The threshold needs to be defined to achieve good performance.

There are also some digital filters, such as the matched filter and low-pass filter to get the heartbeat signal, but they may suppress vital sign signals [26].

2.2.3. IMPACT OF DIFFERENT ORIENTATIONS OF TARGETS

In realistic indoor healthcare applications, in which the orientation of people toward the antenna is typically unknown. So, the performance of scenarios in different orientations should be tested. Sacco et al. [22] considered four orientations of people with respect to the radar, including the back side, front side, left side, and right side. Radar data was compared with the signals measured by a PPG. Results from four scenarios show that respiratory rate and heartbeat can be accurately estimated.

Wang et al. [32] also conducted these four scenarios. It was found that the front side can get the most accurate respiration rate, and the heartbeat has the lowest error on the front side. According to statistical analysis of the data collected from the five people, the

radar can measure respiratory rate and heart rate with high accuracy, regardless of the orientation of the chest towards the antenna.

Ren et al. [33] proposed a derivative independent component analysis (DICA) method to estimate the heartbeat and respiratory using an SFCW radar system with one transmitter and four receivers. This method can not reconstruct the information on the signal amplitude. The data from the front, left, right, and back sides are measured and processed. The errors of heartbeat rate estimation are lower than 3%.

The single input and single output FMCW radar with a 5.8 GHz band was used to measure the left, back, and right sides of heartbeat rate by Sacco et al. [34]. The error on the front side is the lowest, and the error on the right side is the highest [34].

Ren et al. [35] compared the electromagnetic scattering model simulation results and experimental results measured by SFCW radars. Six orientations are analyzed including right 45°, back, front, right 90°, left 45°, right 45°, and left 90°. The first three sides have errors less than 3%, and the left side has the highest error 5.7% because of the lower radar cross section [35].

The three-layer artificial neural network model was used to predict heartbeat by Iyer et al. [36]. The heartbeat data was measured by the FMCW radar at 77GHz with a bandwidth of 4 GHz and Fourier series analysis was applied to extract the phase [36]. The results concluded that the right and left sides did not work well, and the performance is good for the front and back sides [36].

Nahar et al. measured the scenarios putting the targets at 0°, 45°, 90°, and -45° with respect to the radar [37]. An SFCW radar system working at 1 GHz bandwidth was implemented. An electromagnetic (EM) model of scenarios was developed. The errors of heartbeat are less than 2.5% based on the simulation and experiment results [37]. The larger radar cross section will lead to less error was proved in both measurements and simulations [37].

2.2.4. HEARTBEAT ESTIMATION

The existing radar-based heartbeat estimation approaches utilized in papers are described below. The vital sign contains both heartbeat and respiration activities, the heartbeat signal is the desired signal and should be separated.

Lazaro et al. [38] used an impulse radio ultra-wideband (IR-UWB) radar operating at 5GHz to detect the signal. The heartbeat and respiration frequencies are estimated in the normalized spectrum by chirp Z-Transform which can provide a high-resolution analysis [39]. moving target indicator (MTI) removes the respiration frequency from the original signal and then searches for the heartbeat rate [38]. But if the heartbeat frequency is close to the respiration frequency, then the filter may remove the heartbeat along with the respiration [38].

wavelet independent component analysis (WICA) which combined the wavelet decomposition and independent component analysis (ICA) was presented by Mercuri et al. [40]. Phase-Tracking CW Doppler radar at 5.8 GHz detects the chest displacement. Lowpass and highpass filters were used to decompose the signal into low and high-frequency components, then the mother wavelet, which had a similar shape to the signal processed, was used to determine the decomposition level. The ICA method can separate independent sources from the heartbeat and respiration. The shape of the Mother

Wavelet should be selected to be close to the signal.

Weishaupt et al. [6] used empirical mode decomposition (EMD) to decompose the signal into physically meaningful components called intrinsic mode functions (IMF). The raw data measured by Linear frequency modulated continuous wave radar at 76.5GHz is preprocessed to extract the phase containing the respiration and heartbeat signal. EMD is a part of the Hilbert-Huang transform (HHT) and can do convenient frequency estimation [41]. It works like a filter bank. Selecting and summing the appropriate IMFs and components can reconstruct the heartbeat signal. EMD method can extract heartbeat components from the signal generated in noisy nonlinear and nonstationary processes. But this method also has problems, such as mode mixing due to signal interference [42].

Dragomiretskiy et al. [43] proposed the variational mode decomposition (VMD) method which is more robust to sampling and noise compared with the EMD method. It is improved with the alternating direction method of the multipliers approach using 5.8GHz FMCW radar. VMD method cannot be applied in the non-stationary signal directly and the number of modes should be defined at the beginning. Wu et al. [44] combined finite impulse response filter (FIR), comb filter, and VMD algorithm. The improved system is robust to the non-stationary clutter and has a lower computational load and higher SNR than the EMD method. It had higher heartbeat extraction accuracy than the FFT method.

Mikhelson et al. [45] combined the wavelet multi-resolution decomposition method and the statistical algorithm (WMRDS) with a 94-GHz millimeter-wave sensor. The wavelet multi-resolution decomposition method decomposed the displacement signal and has a good time resolution for heartbeats but does not work for every heartbeat [46]. So the statistical algorithm helps to compensate temporal locations of heartbeat obtained from the wavelet method [45].

Tariq et al. [47] detected the phase difference caused by the chest movement by phase-modulated Doppler radar to estimate heartbeat frequency. The wavelet transform (WT) was applied with a good frequency resolution at low frequencies and was suitable for the heartbeat signal with change over a short time. This method can help detect the heartbeat rate without filtering noise when the distance between the radar and the target is close [47]. But if the distance is larger than 1m, the extraction accuracy of the heartbeat signal is not reliable enough, the technology for clutter removal should be added [47].

The breathing and heartbeat rate have different frequencies and can be separated by the bandpass filters applied by Ahmad et al. [48]. The FMCW with a carrier frequency of 77 GHz is used to detect the phase of the chest movement. The frequency of the peak in the spectrum after selection by the signal power threshold is defined as the respiration frequency. The heartbeat frequency is estimated using a density-based approach in the spectrum. Wang et al. [32] also used a bandpass filter and adaptive peak detection after FFT to separate and calculate heartbeat and respiration frequencies.

Birsan et al. [49] used the Doppler radar operating at 24 GHz to measure the chest displacement due to the heartbeat. The Gabor transform (GT) is used to get high accuracy in counting the heartbeats in the time-frequency domain. Gabor transform applied the Gaussian window to get the best time-frequency product among window functions

[50]. Even if there is a big displacement of the target's chest, this method also had a low error. It is hard to reduce the influence of the micromotion dynamics, the fit pattern needs to be found.

The heartbeat and respiration activities are periodic sinusoidal movements with frequencies. Li et al. [51] used Doppler radar to detect chest displacement and process the periodogram by the relaxation approach (RELAX). It can reduce the effects of smearing and leakage problems of the simple periodogram approach but needs more computation [51].

The auto-regressive algorithm (AR) was proposed by Lee et al. [52] to extract the periodicity of the vital signs of multiple targets by the FMCW Doppler radar of 24 GHz. The MUSIC algorithm completed the beat frequency containing range information, and the Fourier transform method was used to phase history extraction. The short-time autoregressive algorithm extracted heartbeat and respiration signals in real-time. It resolved the problem of the range resolution of multiple people estimation, but the algorithm is not robust for small body movements [52].

Kalman filter (KF) based approach was applied by Rahman et al. [53] to the vital sign monitoring using 2.4 GHz Doppler radar. This estimator was used for quadrature signals in the linear dynamic system influenced by white noise [54]. Then principal component combining (PCC) is used to combine the estimated signal. This approach is robust to environmental noise. The extended Kalman filter (EKF) method proposed by Rahman et al. [55] is a non-linear dynamic model extension of KF which is more suitable for vital sign estimation. The phase noise and delay needed further improvement. Kalman filter-based tracking algorithm (KFT) was proposed by Arsalan et al. [56]. The fourth-order Butterworth filter is applied to extract the heartbeat signal from the displacement of the chest surface adaptatively.

The phase FFT proposed by Anitori et al.[57] using FMCW radar st 9.6GHz. The range bin 12 in the range-slow time map is selected to estimate the heartbeat frequency. The range bin with the highest reliability is selected to estimate the respiration frequency in the spectrum using FFT. The heartbeat frequency can be successfully estimated, but with high error.

2.3. SUMMARY

This chapter introduces the physiology of cardiopulmonary activity and its simulation model. For the tests of the impact of the different orientations in some papers, it was found that normally the front side has the highest heartbeat estimation accuracy. The flow of a general processing pipeline typical of all reviewed literature has mainly four blocks shown in 2.4. There are many existing approaches that are studied in this chapter. In the processing pipeline proposed in this thesis, the selected ideas from the analyzed literature will be assembled together for the tasks of clutter removal, RBM cancellation, and heartbeat frequency estimation.

For clutter removal, the existing approaches in Section 2.2.2 are summarized in Table 2.3. The approach which subtracts the DC component in slow time is applied. Because in this project the test people are seated on a chair without large movements like walking, it can help to remove all the stationary objects in the room like the furniture, other parts of the human body besides the chest, the wall, and so on. Since the range bin with

vital sign signals in slow time needs to be selected to estimate the heartbeat frequency, reducing the clutter in slow time can help make it easier to be detected by the maximum variance. This method does not cost too much complex computation compared with other methods such as the loopback filter.

After detecting the range bin, the large-scale random body movement should be detected and canceled. The methods described in Section 2.2.4 are summarized in Table 2.2. For this part, the following three bullets can be derived:

- The multi-radars make the system complex and hard to work synchronously. The extra devices like cameras are non-invasive for indoor healthcare at home. The single FMCW radar which can measure chest displacement to extract the phase history difference of the vital signs is used in this thesis project.
- The heartbeat signal is weak, and using filters will suppress the signal. The lower SNR caused by the method of curve fitting will reduce the phase sensitivity according to the paper [48]. The energy threshold is an effective and simple way to distinguish the RBM.
- The RBM is much larger than the chest displacement due to the vital sign. The energy of the RBM is higher than the normal heartbeat signal. Because the heartbeat frequency of the people may not be valuable for the disease diagnosis when people are not stable, the data with RBM can be discarded.

According to the analysis above, the energy threshold method shown in Table 2.2 is selected to remove RBM in this thesis. Based on simulations and experimental results, the threshold value of the vital sign signal containing RBM will be determined.

For heartbeat frequency estimation, there are lots of approaches in Section 2.2.4. The types of equipment, advantages, and disadvantages of approaches are organized in Table 2.1. The wavelet transform is selected for the heartbeat estimation, because it has a good frequency at low frequencies and the heartbeat frequency is between 1-3Hz which is low. It can help filter the noise when test people are close to the radar. Also, the heartbeat and respiration signals can be separated by multi-resolution analysis of Wavelet transform.

Method	Advantage	Disadvantage	Radar
MTI [38]	high resolution	remove heartbeat signals close to respiration siganl	5GHz IR-UWB radar
WICA [40]	extract the heartbeat and respiration simultaneously	empirical mother wavelet selection	5.8 GHzPhase-Tracking CW Doppler radar
EMD[58]	nonlinear signal analysis	sensitive to noise and sampling	/
VMD [43]	more robust to sampling and noise	can not be applied in the non-stationary signal directly and need the defined the number of the modes	/
WMRDS [45]	good time resolution	does not work for every heartbeat, and complex system	94-GHz millimeter-wave sensor
WT [47]	good frequency and time resolution	lower accuracy at lager distances	Doppler radar
bandpass filters and density-based approach[48]	influenced by random body movements	remove noise from surrounding clutter	77 GHz FMCW Radar
GT [49]	preserve physical uniqueness of decomposition, high accuracy in the time-frequency domain	influenced by the micromotion dynamics, the fit pattern should be found	24 GHz Doppler radar
AR [52]	resolve the range ambiguity and has a high resolution	not robust for small body movements	24 GHz FMCW Radar
KF [53]	robust to environmental noise	linear dynamic system	Doppler radar
EKF [55]	non-linear dynamic model	phase noise and delay	Doppler radar
KFT [56]	remove random body movements	needs more computation	60GHz FMCW radar with the bandwidth of 2 GHz
phase FFT [57]	take into account bandwidth availability	fixed range bin	9.6 GHz FMCW radar

Table 2.1: Summary of the main studies in the literature on radar-based approaches for heartbeat estimation

Method	Advantage	Disadvantage	Radar
AC [25]	reduce unreliable measurements	may lose some information	IR-UWB radar
AKF [26]	can work without training data and have good performance when the movement changes	have model fitting error	Garmin belt
MDM [27]	cancel out strong noise	complex system with multiple radars synchronized	two 5–6 GHz portable radars
MSM [59]	effectively reduce RBM	complex measurement	Doppler radar and camera
CF [29]	reconstruct signal from strong body movement noise	low SNR	continuous wave Doppler radar
ARA [30]	clear peaks of the heartbeat and respiration	complex measurement	two incoherent FMCW radars
energy threshold [31]	simple and effective for large-scale movement	threshold needs to be defined	77–81 GHz FMCW radar
digital filters [26]	simple system	suppress the vital sign signals	/

Table 2.2: Summary of the main studies in the literature on approaches for Random body movement cancellation

Method	Advantage	Disadvantage	Radar
moving averaging filter [20]	achieving the breathing signal with a SNR	window length selecting	UWB radar
moving averaging filter added a weighted factor [21]	emphasizes recent events	computationally complex	UWB sensor networks
standard deviation over slow time [22]	the subject can clearly be distinguished from static objects	/	FMCW radar operating in the 5.8 GHz
SVD [23]	/	not work for all kinds of materials	UWB radar
loopback filter [24]	good background subtraction	/	IR-UWB radar

Table 2.3: Summary of the main studies in the literature on approaches for clutter removal

3

PROPOSED PROCESSING PIPELINE DESIGN

In this chapter, a processing pipeline is proposed inspired by the ideas from the literature review. In section 3.1, the working principle of FMCW radar and the design of the waveform is illustrated. Section 3.2 explains in detail the main blocks and steps of the proposed processing pipeline.

3.1. FMCW RADAR AND WAVEFORM

3.1.1. PRINCIPLE OF FMCW RADAR

The Frequency Modulated Continuous Wave Radar (FMCW) radar is a type of radar sensor that can radiate power continuously and modulate the frequency of the transmitted signal. The frequency modulation of the radar used in this project is linear sawtooth frequency modulation. The shape of the chirp is shown in Figure 3.2. The radar sends the signal continuously and receives the echo signal reflected by the objects. The delay between the transmitted and received signal results in the frequency shift, which is the beat frequency, the model of the beat signal is shown in Equation 2.9. The radar transmits chirps every chirp time. The range of the target can be detected by the delay between the transmitted and the received signal. The Doppler frequency of the target can also be measured by the frequency difference between the transmitted and the received signals.

3.1.2. WAVEFORM DESIGN

The Texas Instrument (TI) mm-wave radar IWR6843 with a carrier frequency of 60GHz is chosen. The radar system is shown in Figure 3.1.

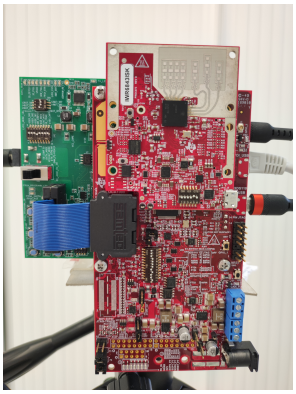

Figure 3.1: Texas Instrument (TI) mm-wave radar IWR6843 together with the acquisition board used in this thesis project

The configuration of a single FMCW chirp in the time domain is shown in Figure 3.2. The chirp time includes the idle time, which is required for the radar to decrease the end frequency to the start frequency, and the ramp time. The frequency slope of the chirp is determined by the bandwidth and ramp time. The settings of two types of waveform designed are summarized in Table 3.1. Waveform 1 (W1) was designed by Irving Maximino Cortés Peralta to measure joint human motion and breathing frequency [1]. It is proved that it can capture respiration activity. In this project, the settings of the waveforms designed should be capable of measuring the heartbeat activity. Waveform 2 (W2) is designed in Section 5.2.1 to fit the sitting scenario tested in this project. Both two waveforms are able to measure the heartbeat and respiration activities.

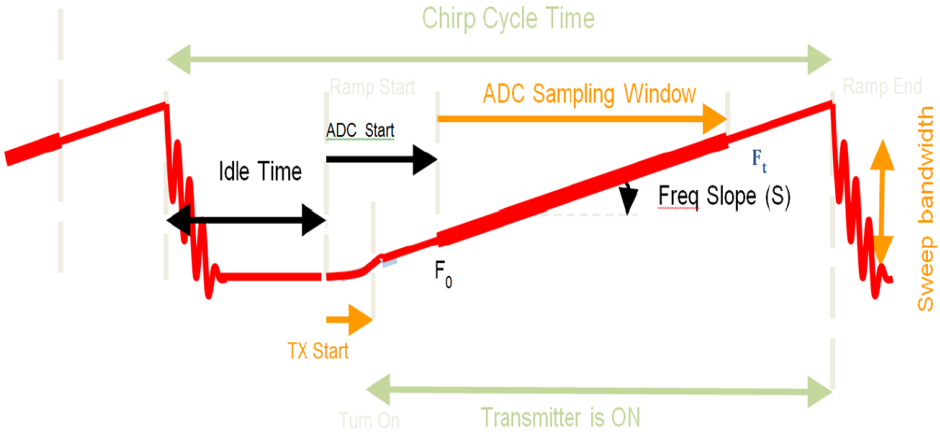

Figure 3.2: Single chirp and related parameters from TI IWR6843 radar [60]

Radar parameter	Waveform 1	Waveform 2
Carrier Frequency [GHz]	60	60
Frequency Slope [MHz/us]	30	60
Number of ADC samples per chip	128	128
ADC start time [us]	6	6
Ramp Time [us]	100	100
Idle Time [us]	5160	3800
Chip Duration [us]	5260	3900
Number of chirps per frame	255	255
Frame Duration [s]	1.341	0.9949
Bandwidth [MHz]	3000	3000
Range Resolution [cm]	5	5
Unambiguous Range [m]	6.4	6.4
Unambiguous frequency [Hz]	95.057	128.205

Table 3.1: Radar parameters of Waveform 1 from previous work [1] and Waveform 2 designed in this thesis project

The FMCW radar detects the propagation delay to compute the displacement of the chest surface. Range and Doppler resolution and ambiguity should be checked if respiration and heartbeat activity can be recognized.

The Doppler frequency resolution determines the minimum Doppler frequency change that the radar can detect. It can be derived by equation 3.1. The interval is the observation time of measurement data processed in the algorithm to output a heart rate frequency. The minimum length of the interval is 2 s because the wrist oximeter captures the ground truth heartbeat frequency every two seconds. So the maximum value of the Doppler frequency resolution is 0.5Hz in this thesis project. The influence of the length of the intervals on the estimation error is discussed in Section 4.2.

$$\Delta f = \frac{1}{MT_{chirp}} \tag{3.1}$$

Here, T_{chirp} is the chirp time, and M is the number of chirps in one interval in the algorithm which is the observation time.

The unambiguous frequency is calculated by Equation 3.2. The unambiguous frequency of Waveform 1 and 2 is 95.057Hz and 128.205Hz respectively, which is higher than the maximum heartbeat frequency.

$$f_{\max} = \frac{1}{2T_{chirp}} \tag{3.2}$$

The range resolution can be derived by Equation 3.3. The maximum displacement of the chest due to the heartbeat and respiration is 11mm which is lower than 5cm and can be detected in one range bin. Because the target is not multiple in this project, the range resolution is not considered for the target distinction. But if there are random body

movements, a higher range resolution can help to separate vital signs and RBM.

$$\Delta R = \frac{\mathrm{c}}{2B} = \frac{3 \times 10^8}{2 \times 3 \times 10^9} = 0.05m = 5cm \tag{3.3}$$

Here, B is the bandwidth of the radar, and c is the speed of the light.

The unambiguous range can be derived by Equation 3.4. The initial range between the radar and the target is defined as shorter than the unambiguous range.

$$R_{\max} = N_{ADC}\Delta R = 128 \times 0.05 = 6.4m \tag{3.4}$$

Here, N_{ADC} is the number of ADC samples in one chirp.

In conclusion, the ambiguity and resolution of range and frequency are essential parameters in waveform design. The range and frequency of the chest displacement should be below the unambiguity range and frequency. Otherwise, the reflected signal from the chest can not be received before the next transmitted chirp to get the correct frequency information of the target. The range and frequency resolution of the FMCW radar determines the minimum range and frequency that the radar can detect. The phase history difference is used to estimate heartbeat frequency because the range resolution of the radar utilized in this thesis project can not achieve the measurement of millimeters. Then Doppler frequency resolution is a crucial parameter to the accuracy of the heartbeat estimation. It is determined by the length of the observation intervals, which is discussed in the simulation and experimental data analysis.

3.2. PROPOSED PROCESSING PIPELINE DESIGN

The processing pipeline describes the detailed steps of how the algorithm processes the radar raw data to the heartbeat frequency. There are two main parts including the extraction of the phase history difference and the estimation of the heartbeat frequency.

3.2.1. EXTRACTION OF THE PHASE HISTORY DIFFERENCE

The processing steps of extracting the phase history difference are shown in Figure 3.3. The raw data is read from the FMCW radar, it needs to be reshaped to the samples-chirps matrix. The range information of the target is contained in fast time over samples at each chirp. The frequency (velocity) information of the target movement is contained in the slow time domain over the chirps. The range-slow time map is generated after applying Fourier transform over samples at each chirp. The clutter noise of reflections from stationary objects can be removed by subtracting the average power over the slow time.

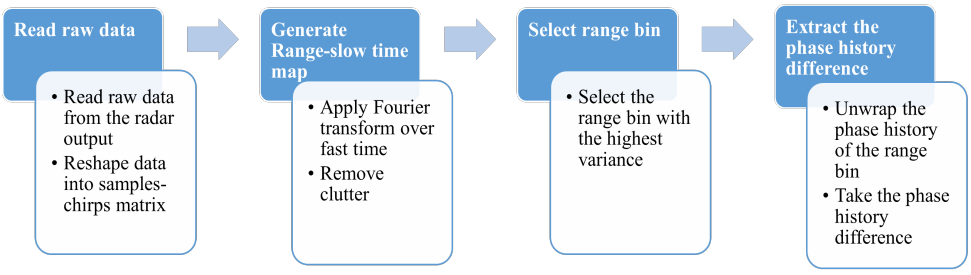

Figure 3.3: Extraction of the phase difference in the proposed processing pipeline

The highest reflected power occurs at about 0.5m, which is the initial distance between the chest of the target and the radar in Figure 3.4. The received power is inversely proportional to the fourth power of the range. The influence of the range is not studied in this thesis project. The variance over the chirps is derived, and the range bin with the highest variance contains the vital signs. Because the other objects in the range map are stationary, and the chest has movement due to heartbeat and respiration activities will result in a higher variance. The phase history of the range bin is unwrapped to remove the influence of the initial distance between the radar and the chest. The phase history difference is calculated by subtracting the sequential phase history to strengthen the heartbeat signal for further frequency estimation.

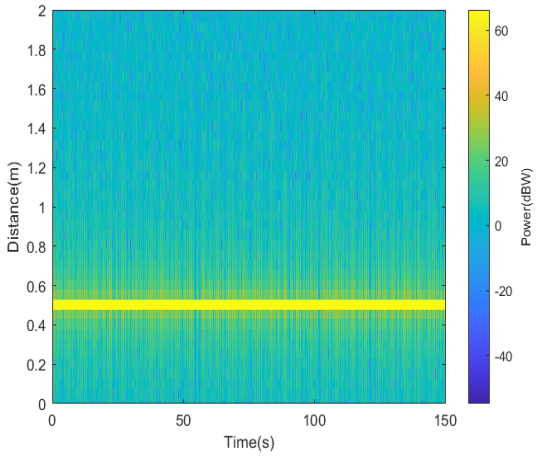

Figure 3.4: Range-slow time map when the target is seated at 0.5m away from the radar without RBM

3.2.2. ESTIMATION OF HEARTBEAT FREQUENCY

The processing steps of heartbeat frequency estimation are shown in Figure 3.5. The intervals with RBM are detected and discarded according to the energy level of the phase history difference, and the detailed steps are described in Section 3.2.3. The measurement length is split into observation intervals of the same time length. The wavelet

transform is applied to each observation interval and decomposes it into multi-levels with different frequency bands by wavelet transform. Selecting suitable levels can help to filter out the heartbeat and respiration signals. The principle of the wavelet transform is explained in Section 3.2.4.

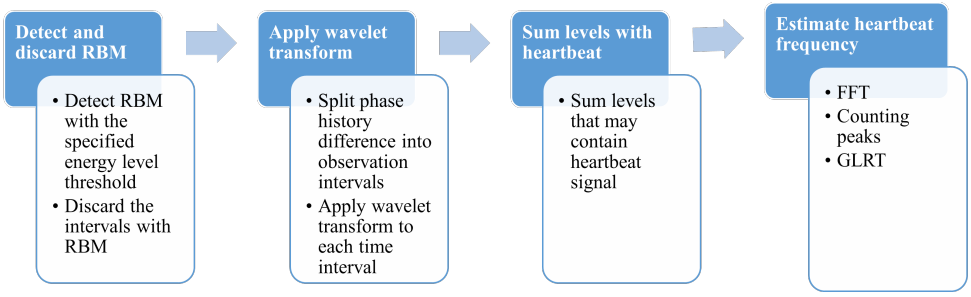

Figure 3.5: Estimation of heartbeat frequency after extracting the phase history difference in the processing pipeline shown in Figure 3.3

Two methods to select needed levels with heartbeat were tested. The first method is to select the level with the highest auto-correlation peak because the heartbeat signal is periodic and the auto-correlation can help verify the presence of periods. The second method is summing all levels that may contain the heartbeat signal. The heartbeat frequency is about 1-3Hz according to the literature. For example, if the chirp time is 5260us, then the fifth, sixth, and seventh levels have the frequency band of 2.97-5.94Hz, 1.49-2.97Hz, and 0.74-1.49Hz. These three levels may contain the heartbeat signal, so the algorithm directly sums them up for heartbeat estimation. The performance of the auto-correlation method is not good because the respiration activity is also periodic and the heartbeat is not perfectly periodic in experimental data, so the method of summing levels is assembled in the final processing pipeline.

After getting the heartbeat signal by wavelet transform, there are three methods to calculate the heartbeat frequency of each observation interval in the time or frequency domain. The FFT method applies the second Fourier transform over slow time and selects the frequency with the maximum amplitude as the heartbeat frequency in the spectrum.

The other two methods count the heartbeat frequency in the slow-time domain. The second method is counting the number of peaks of the heartbeat signal and dividing the number by the length of the observation intervals to get the heartbeat frequency. For example, the heartbeat signal of one observation interval of 2 s is shown in Figure 3.6. There are four peaks, and then the heartbeat frequency is 4/2=2 Hz.

The third method combines the second method and the generalized likelihood ratio test (GLRT) proposed in [45]. The samples within 1/4 of the distance from the peak are defined as having a heartbeat, while the rest are defined as having no heartbeat. Figure 3.6 shows the heartbeat and non-heartbeat selection selection. The red points are defined as points with the heartbeat (HB), and the green asterisks correspond to points without the heartbeat (nHB).

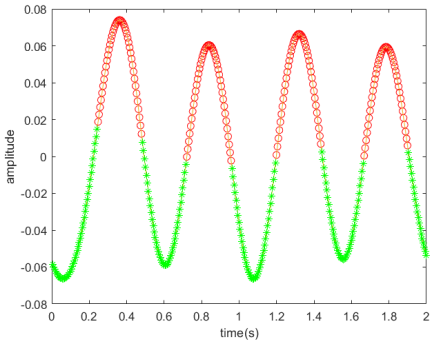

Figure 3.6: Heartbeat(red) and non-heartbeat(green) selection for further heartbeat frequency estimation using GLRT method

The histogram of two types of points is shown in Figure 3.7 and is fitted to the normal distribution. The amplitude of the first intersection of the distributions is defined as the threshold for deciding whether the peak contains a heartbeat. The total number of heartbeat peaks in the observation interval is counted using the counting peaks method. The peaks that have lower amplitude than the threshold are subtracted from the counted number. Then, the heartbeat frequency can be calculated by dividing the number of heartbeat peaks by the length of the observation interval.

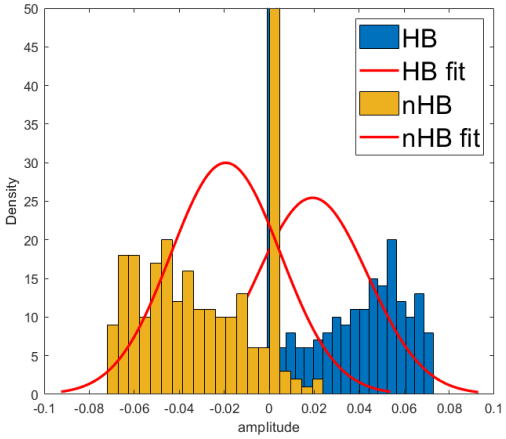

Figure 3.7: Histogram of HB and nHB values and fitted distributions from Figure 3.6 using GLRT method

3.2.3. RANDOM BODY MOVEMENT CANCELLATION

The random body movement is detected by the energy level of the phase history difference and the observation intervals with RBM are discarded. Numerical integration via the trapezoidal method is used in the algorithm to calculate the energy level which is equal to the area between the phase history difference and the time axis.

The threshold is determined by comparing the energy level when there is an RBM and no RBM. When the energy level is higher than the threshold times the energy level of the previous segment, this time interval is judged to have an RBM. The detection flow is shown in Figure 3.8. After the measurement length is split into intervals, the energy of the observation intervals is calculated. The energy of the evaluated interval is defined as eng1. If it is higher than the threshold multiplied by the energy of the previous one interval before the evaluated interval eng2, the evaluated interval is defined as having RBM and discarded. Then, the following interval eng3 will also be compared with eng2 until one interval is defined as no RBM.

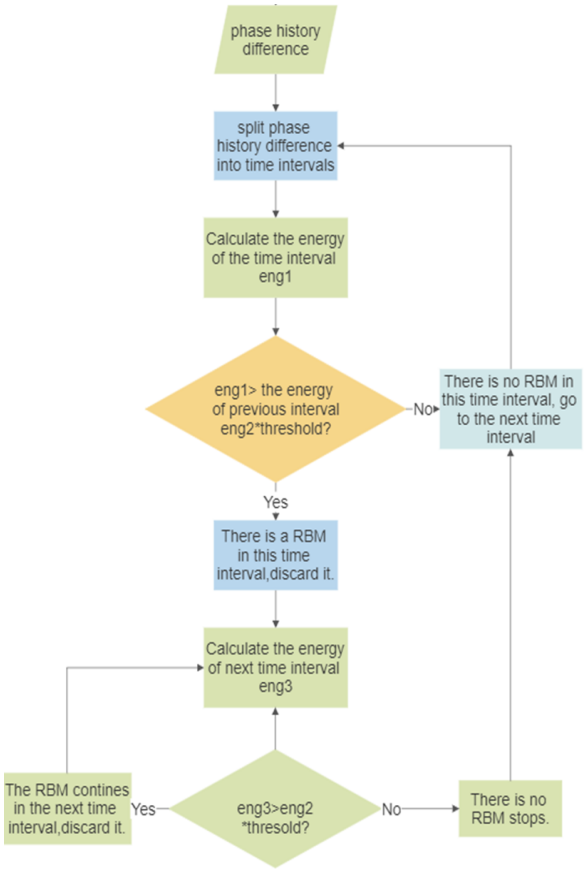

Figure 3.8: The RBM detection flow in the proposed pipeline

3.2.4. WAVELET TRANSFORM

Discrete wavelet transform (DWT) has been applied in processing biomedical signals like ECG signals in the time and frequency domain [61]. The Fourier transform has a good frequency resolution but no time resolution. The Short Time Fourier transform divides the signal into the same length by a sliding window and then applies the Fourier

Transform. The time and frequency resolutions are fixed and determined by the length of the window. The wavelet transform can decompose a signal into different frequencies by multi-resolution. The multi-resolution analysis of wavelet transform has good frequency resolution and poor time resolution at low frequencies and has good time resolution and poor frequency resolution at high frequencies. The equation of the wavelet transform applied to a signal X(t) is shown in Equation 3.5.

$$X(\tau, s) = \frac{1}{\sqrt{|s|}} \int_{-\infty}^{+\infty} X(t)\varphi^*(\frac{t-\tau}{s})dt \tag{3.5}$$

Here, s is the scale parameter that defines how it stretches and compresses the wavelet. τ is the translation parameter that defines how the wavelet translates across the signal. φ is the wavelet function.

The Maximal Overlap Discrete Wavelet Transform (MODWT) implemented by the existing function in MATLAB in this thesis project is the modified version of the DWT [62]. It performs the decomposition of the signal into wavelet and scaling coefficients with a filter bank of high-pass and low-pass filters [63], shown in Figure 3.9. This does not discard samples after every decomposition like DWT, which is suitable for the short observation intervals of the heartbeat signal. The maximal overlap property at each level ensures efficient utilization of information across scales compared to DWT [62]. After applying different types of wavelets in the algorithm, Daubechies 4 is selected as the wavelet because it has higher accuracy in the heartbeat frequency estimation.

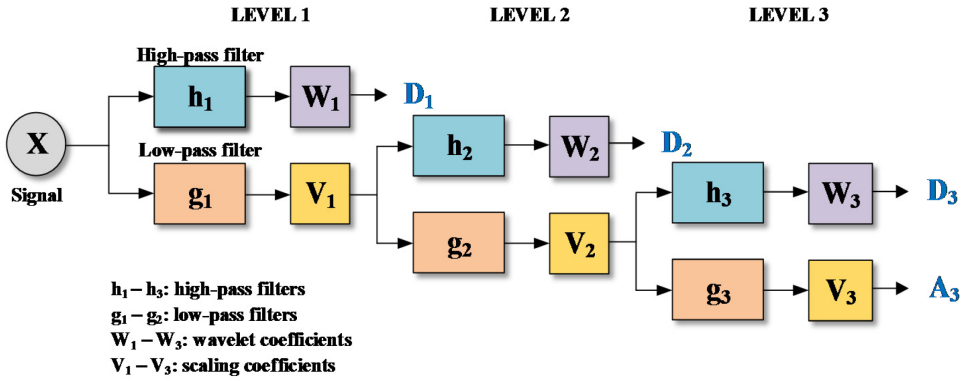

Figure 3.9: MODWT decomposition tree [63]

The wavelet and scaling filters are defined in Equation 3.6 [64].

$$\tilde{h}_{j,l} = h_{j,l}/2^{j/2}, \tilde{g}_{j,l} = \tilde{g}_{j,l}/2^{j/2} \tag{3.6}$$

where $h_{j,l}$ is the DWT wavelet filter of length l and jth level decomposition, $g_{j,l}$ is the scaling filter of length l and jth level decomposition. l=1,2,..., L is the length of the filter, and j is the level of decomposition.

The wavelet coefficient $W_{j,t}$ and scaling coefficient $V_{j,t}$ of jth level are defined as the convolution of time series X and MODWT filters in Equation 3.7 [64].

$$W_{j,t} = \sum_{l=0}^{L_j-1} \tilde{h}_{j,l} X_{t-l \bmod N}, V_{j,t} = \sum_{l=0}^{L_j-1} \tilde{g}_{j,l} X_{t-l \bmod N} \tag{3.7}$$

where $X = \{X_t, t = 0,1,2,...,N-1\}$ is the time series of the original signal,and $L_j = (2^j - 1)(L-1)+1$

The inverse transformation can reconstruct the original signal from the wavelet and scaling coefficients. The multi-resolution analysis (MRA) component of the jth level MODWT details of the signal X corresponds to different frequency bands [64]. The frequency band is defined by the level of the MRA component and sampling interval, which is the chirp time of the FMCW radar measuring the vital sign signal in this thesis project. The phase history difference extracted to estimate the heartbeat signal is in the slow time domain over sequential chirps. So the frequency band of MRA components in the jth level is defined by Equation 3.8.

$$[\frac{1}{2^{j+1} T_{chirp}}, \frac{1}{2^j T_{chirp}}] \tag{3.8}$$

where T_{chirp} is the chirp time of the FMCW radar used to measure the vital sign signal in this thesis project.

3.3. SUMMARY

This chapter proposes the processing pipeline for heartbeat estimation formulated and validated in this thesis project. The phase history difference is selected for the heartbeat frequency extraction from the chosen range bin in the Range-slow time map. The time intervals with RBM are detected and discarded by the energy level threshold. Wavelet transform decomposes the heartbeat signal from the phase history difference containing the vital signs. Then, the heartbeat frequency is estimated with three approaches, either through the frequency domain by the FFT method or through the time domain by counting peaks or GLRT methods. The performance of the processing pipeline to heartbeat frequency estimation and RBM cancellation are validated and analyzed by the simulations and experiments in Chapter 4 and Chapter 5.

4

SIMULATION RESULTS AND ANALYSIS

The processing pipeline described in the previous chapter is validated in this chapter via numerical simulations implemented in MATLAB and following a Monte Carlo strategy to simulate possible different scenarios. The influence of different lengths of observation intervals is analyzed in Section 4.2. The algorithm for RBM cancellation is tested in Section 4.3. The ability to estimate the respiration frequency is also studied in Section 4.4. For conciseness, the discussion of the orientation simulation and overlap percentages are shown in Appendix 7.

4.1. HEARTBEAT FREQUENCY ESTIMATION METHODS

Multiple scenarios with constant and non-constant heartbeat frequencies are simulated to evaluate the performance of the heartbeat frequency estimation. The simulation with the constant heartbeat frequency can verify whether the algorithm will react differently to different heartbeat frequencies between 1-3 Hz. There are 100 data sets with constant heartbeat frequencies from 1 to 3Hz. The amplitude of heartbeat and respiration and the frequency of respiration are random. The simulation with the non-constant heartbeat has heartbeat frequency changing during the measurement time, which can help to check whether the algorithm is robust to rising and falling or mutating heartbeats. Ten non-constant heartbeat frequency patterns are shown in Appendix 7. The median filter is not used in the simulation because there are not too many impulse-like artifacts in the phase history difference.

Two kinds of errors are used to evaluate the algorithm's performance. The average error in the results is the average value of the errors of all the intervals. The first type of error is defined as the absolute difference between the estimated and ground truth frequency derived in Equation 4.1. This is used to check if the difference between the estimation and ground truth data is related to the magnitude of the ground truth heartbeat frequency.

$$error = \left| f_h - f_{h\_gt} \right| \tag{4.1}$$

Here, f_h is the estimated heartbeat frequency in Hz, and f_{h_gt} is the ground truth heartbeat frequency in Hz.

The second kind of error is the relative error defined by Equation 4.2. It is easier to compare with the error of other estimation approaches based on radars in other papers. The same difference error also has different importance for low and high ground truth frequencies.

$$relative\ error = \frac{\left| f_h - f_{h\_gt} \right|}{f_{h\_gt}} \times 100\% \tag{4.2}$$

Here, f_h is the estimated heartbeat frequency in Hz, and f_{h_gt} is the ground truth heartbeat frequency in Hz.

Three heartbeat frequency estimation methods introduced in Section 3.2.2 including FFT, GLRT, and counting peaks, were applied and compared in the simulations.

Firstly, three estimation methods are applied to the constant heartbeat frequency. Figure 4.1 to Figure 4.6 below shows the average error and average relative error of all people over different ground truth frequencies. The length of the observation interval is set to 2 s.

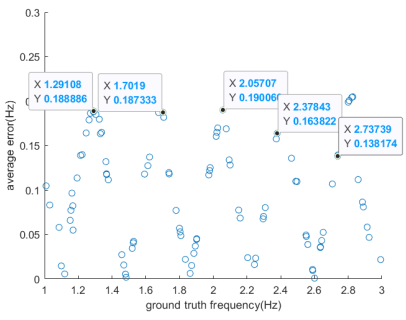

Figure 4.1: Average error of all people over different ground truth heartbeat frequencies(FFT method, simulations with constant ground truth heartbeat frequency pattern)

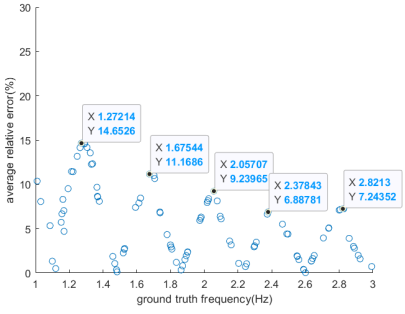

Figure 4.2: Average relative error of all people over different ground truth heartbeat frequencies(FFT method, simulations with constant ground truth heartbeat frequency pattern)

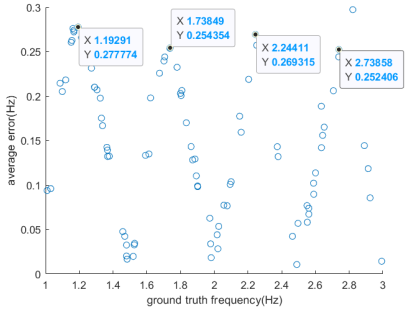

Figure 4.3: Average error of all people over different ground truth heartbeat frequencies(GLRT method, simulations with constant ground truth heartbeat frequency pattern)

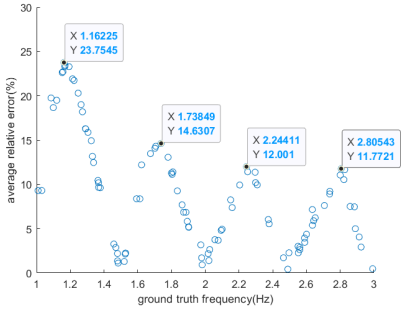

Figure 4.4: Average relative error of all people over different ground truth heartbeat frequencies(GLRT method, simulations with constant ground truth heartbeat frequency pattern)

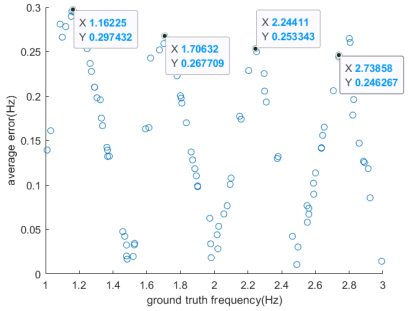

Figure 4.5: Average error of all people over different ground truth heartbeat frequencies(counting peaks method, simulations with constant ground truth heartbeat frequency pattern)

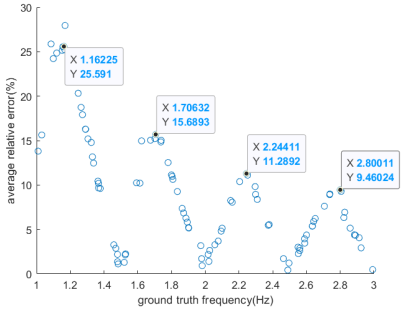

Figure 4.6: Average relative error of all people over different ground truth heartbeat frequencies(counting peaks method, simulations with constant ground truth heartbeat frequency pattern)

The average error of the three estimation methods has the shape of waves with peaks. The amplitude of peaks of average relative errors decreases because the relative errors need to be divided by increasing ground truth frequency. The shape of waves is due to the limitation of Doppler resolution. The different ground truth frequency between two sequential peaks is estimated as the same frequency. The comparison between the estimated and ground truth heartbeat frequency using the FFT method is shown in Figure 4.7. For example, the ground truth frequencies between 1.72Hz,1.87Hz, and 2.03Hz are estimated as the same frequency about 1.85-1.87Hz. The estimation error is lowest when the ground truth frequency is 1.87Hz. When the ground truth frequency is far away from 1.87Hz between 1.72Hz and 2.03Hz, the estimation error is larger.

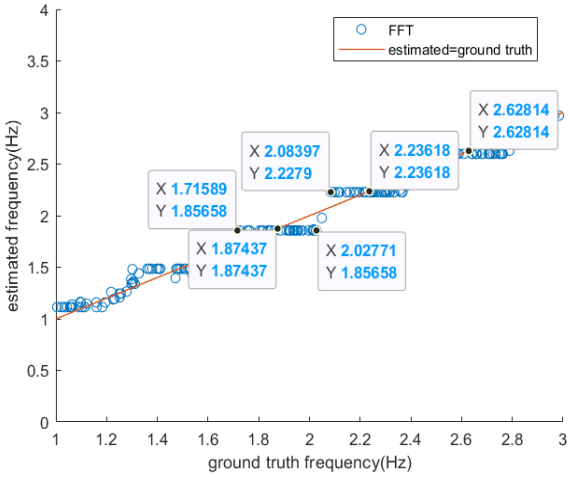

Figure 4.7: Estimated and ground truth heartbeat frequencies(FFT method, constant ground truth heartbeat frequency pattern)

The average ground truth frequency difference between peaks of the FFT method is about 0.38 Hz. The average ground truth frequency difference between the peaks of GLRT and counting peaks methods is about 0.52-0.55 Hz. It is related to the Doppler resolution. The length of the intervals determines the Doppler resolution. The interval length is 2s in this section, the Doppler resolution is 0.5Hz. The frequency interval of the FFT method is a little lower because the heartbeat signal in the frequency domain after FFT is discrete with zero padding in MATLAB, and the selection of the peak point in the frequency domain is not always precisely the peak of the main lobe curve. The selected points may be the closest points on the left or right of the real peaks because of the resolution of the curve.

The maximum relative errors of the FFT, GLRT, and counting peaks methods are about 14.65%, 23.75%, and 25.59%. The FFT method has a lower error than the other two methods. Because the heartbeat frequency is constant, the main lobe with the highest peak in the frequency domain after FFT is dominant and close to the frequency of the heartbeat signal. The influence from the impulse-like artifacts is small and will not shift or hide the main lobe. For GLRT and the counting peaks methods, the heartbeat signal is almost perfectly periodic in simulation. It is easier to count the peaks of the heartbeat activity in the time domain.

The average relative error over different patterns of non-constant ground truth frequencies is shown in Figure 4.8. Three methods have relative errors lower than 17.68% for all types of patterns. The average of average relative errors of all patterns of the FFT, GLRT, and counting peaks methods are 8.56%,15.17%, and 10.99%. The FFT method still has a lower error than the other two methods. The length of the interval is 2s, which is short. Then, the heartbeat frequency does not change too much to generate more sidelobes with peaks with high amplitude in the frequency domain to hide or shift the main lobe of the heartbeat.

The GLRT method has a higher error than counting peaks because of the threshold of

the eliminated peaks. When the time between sequential peaks is lower than 1/3=0.33 s which means the frequency threshold is 3Hz, the peaks are not counted. This threshold is too strict and makes some heartbeat peaks miss detected. After increasing the time threshold to 1/3.5=0.29 s, the GLRT method is improved and has a lower error than the counting peaks method shown in Figure 4.9.

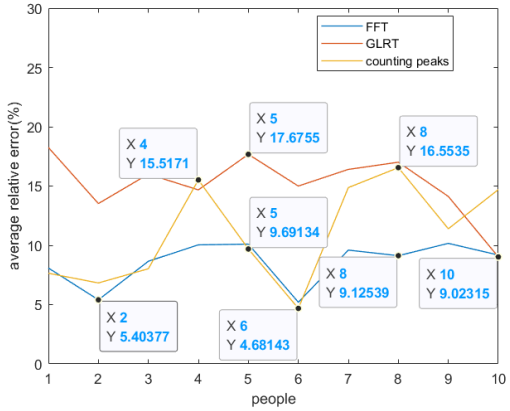

Figure 4.8: Average relative error for different simulated people with non-constant heartbeat frequency pattern (comparison of 3 methods)

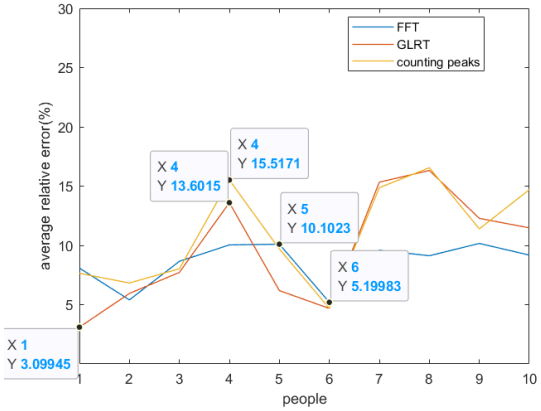

Figure 4.9: Average relative error for different simulated people with non-constant heartbeat frequency pattern (comparison of 3 methods with improved GLRT)

4.2. LENGTH OF OBSERVATION INTERVALS

The length of observation intervals is also called the observation time of the estimation. The observation time is the inverse of the Doppler resolution. When the length of in-

tervals increases to 12s, the Doppler resolution is 0.083Hz, which is much higher than 0.5Hz when the interval is 2 s shown in Figure 4.7.

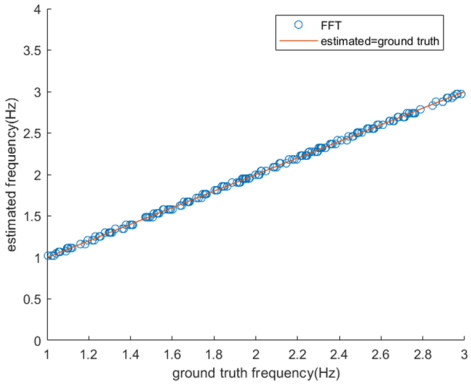

Figure 4.10: Estimated and ground truth heartbeat frequencies(FFT method; observation interval=12s)

Most frequency points shown in Figure 4.10 are very close to the reference line where the estimated heartbeat frequency equals the ground truth frequency because of the higher Doppler resolution. Then the relative error is lower. The simulation results of constant heartbeat frequency over different lengths of observation intervals are shown in Figure 4.11. When the length of the intervals increases, the relative error is lower with a higher Doppler resolution. A relative error lower than 8.37% can be achieved with a short interval of 2s by three estimation methods. After increasing the interval longer than 20 s, all three methods can achieve a relative error lower than 1%.

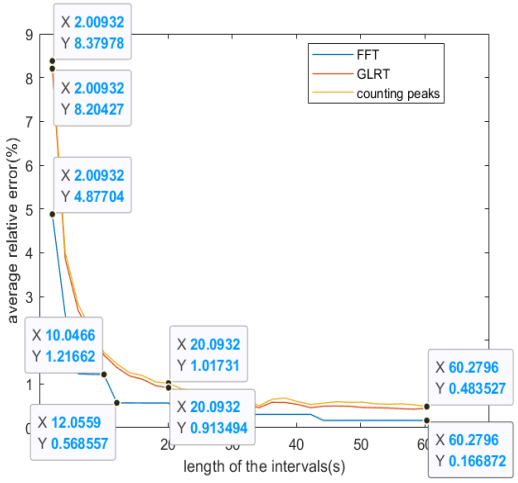

Figure 4.11: Average relative error of all people over different lengths of the observation intervals for three methods (simulations with constant heartbeat frequency)

The simulation results of non-constant heartbeat frequency over different lengths of observation intervals are shown in Figure 4.12. Although the Doppler resolution is higher with longer intervals, the frequency change in one interval is also higher. The

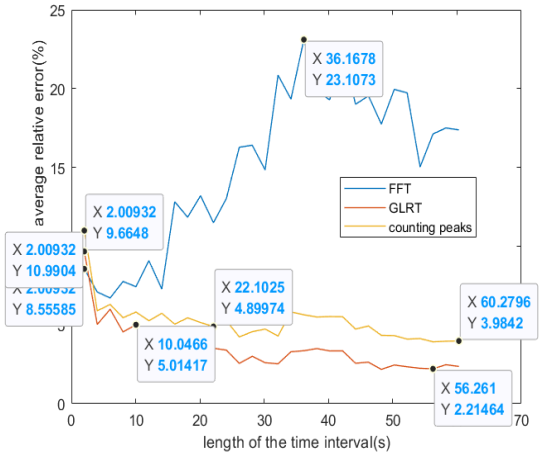

Figure 4.12: Average relative error of all people over different lengths of the observation intervals for three methods (simulations with non-constant heartbeat frequency)

non-constant frequencies generate more sidelobes with high amplitude peaks that hide or shift correct frequency peaks, and then the FFT method has a higher error. For example, the ground truth frequency of one interval changes from 1.4, 1.24 to 1.08 Hz shown in Figure 4.13, and the average frequency is 1.19Hz. The output of one interval of 30s

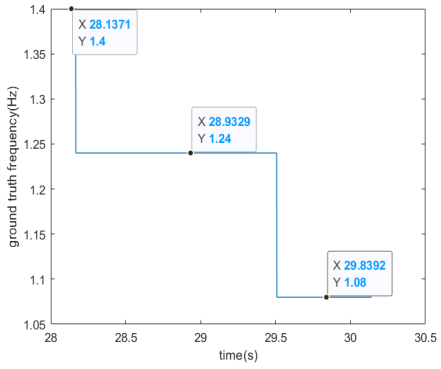

Figure 4.13: Ground truth frequency of one interval using FFT method

using the FFT method is shown in Figure 4.14 in the frequency domain. The selected estimated frequency is 1.49 Hz, which is higher than any frequency defined in this interval, and the desired correct peak is hidden. The error is about 25%, which is high. For

the other two methods, they count the heartbeat activity in the time domain that is not influenced by sidelobes in the frequency domain. The GLRT method has a lower error than the counting peaks method because it eliminates the small and close peaks caused by frequency changes.

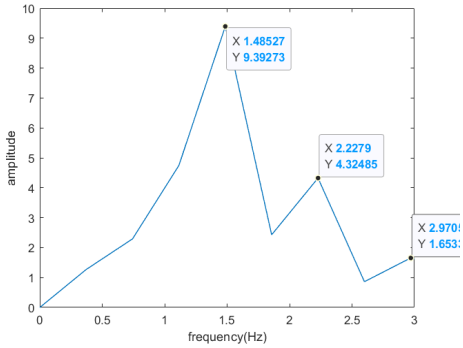

Figure 4.14: An interval in the frequency domain using FFT method for the frequency estimation of Figure 4.13

4.3. RANDOM BODY MOVEMENT CANCELLATION

There are two kinds of movement models used to simulate RBM, such as shaking heads and moving the chest. Both of them are large-scale movements that are much larger than chest displacement due to heartbeat and respiration activities. The energy threshold of the RBM detection is set as 3 after testing different values to detect the intervals with the RBM as many as possible and reduce the false detection. The confusion matrix is used to evaluate the performance of the RBM detection. "1" means the interval has an RBM, and "0" means the interval does not have an RBM.

The first kind of RBM is not periodic and is defined by the velocity. An example of RBM in the time domain of the first kind of RBM is shown in Figure 4.15.

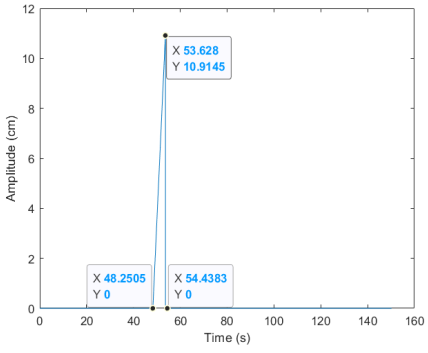

Figure 4.15: Model of RBM 1 over time where the RBM is modeled with constant velocity

The Monte Carlo simulation randomly selects constant velocity between 2-6 cm/s and the RBM 1 occurs in four continuous frames which is about 5s. The confusion matrixes of constant in Figure 4.16. The probability of the correct decision is 97. 6%, which means that most RBM intervals are detected correctly. 109 out of 7021 intervals without RBM are incorrectly detected as intervals with RBM, the false alarm probability is only 1.6%.

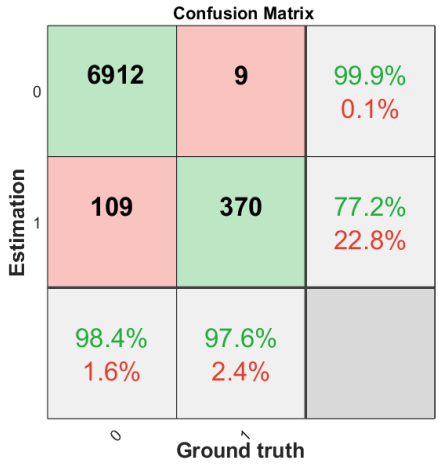

Figure 4.16: Confusion matrix of RBM 1 detection(constant ground truth heartbeat frequency pattern)

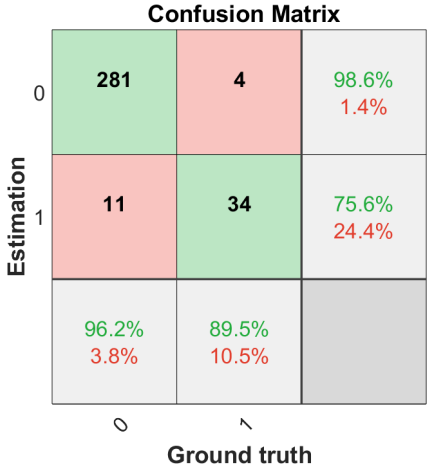

Figure 4.17: Confusion matrix of RBM 1 detection(non-constant ground truth heartbeat frequency pattern)

The confusion matrixes of non-constant heartbeat frequency simulations are shown in Figure 4.17. The probability of the correct decision is 89.5%, meaning most of the

RBM intervals are detected correctly. The false alarm probability is 3.8%. The detection algorithm is effective for the first kind of RBM.

The second kind of RBM shown in Figure 4.18 is periodic with a frequency between 0.5-4Hz, including the frequency band of summed levels after the wavelet transform. The movement is a cosine wave with an amplitude between 2-20cm.

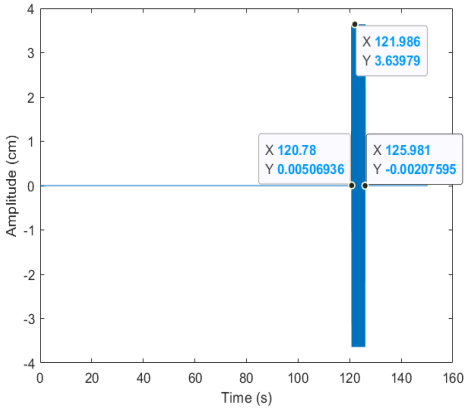

Figure 4.18: Model of RBM 2 over time where the RBM is modeled with frequency

The confusion matrix of constant frequency simulations is shown in Figure 4.19. The confusion matrix of non-constant heartbeat frequency simulations is shown in Figure 4.20. The probability of the correct decision is higher than 98.1%. The false alarm probability is lower than 2.1%. The detection algorithm is effective for the second kind of RBM 2.

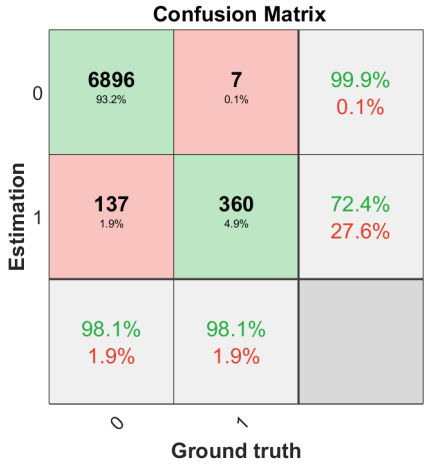

Figure 4.19: Confusion matrix of RBM 2 detection(constant ground truth heartbeat frequency pattern)

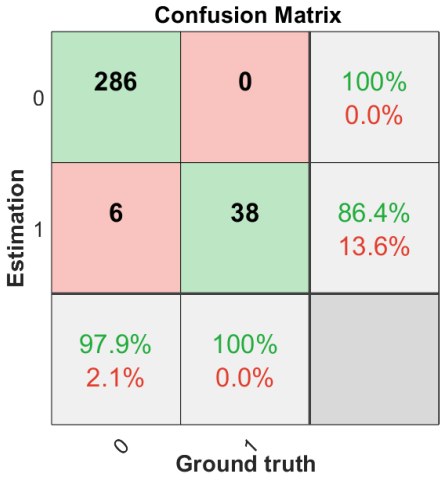

Figure 4.20: Confusion matrix of RBM 2 detection(non-constant ground truth heartbeat frequency pattern)

4.4. RESPIRATION ESTIMATION

The respiration frequency is between 0.1 and 0.3 Hz, and the summed level after the wavelet transform is the 9th level which contains the frequency band of 0-0.37Hz. The period of one respiration activity is between 3.33-10 s, then the time of the interval is defined as 12s to make one interval contain at least one respiration period. The average errors and relative errors of constant respiration frequency over different lengths of intervals are shown in Figure 4.21 and Figure 4.22. The FFT method has a lower error between 1.66% with intervals of 14s and 13.11% with intervals of 60 s than the other two methods. The counting peaks method has the highest error. The accuracy is higher with longer intervals because of the higher Doppler resolution.

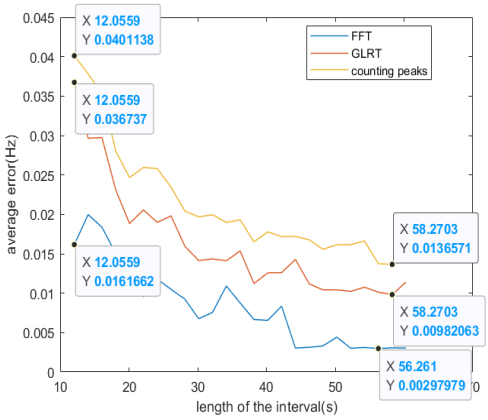

Figure 4.21: Average error of all people over different lengths of the intervals(constant ground truth heartbeat frequency pattern)

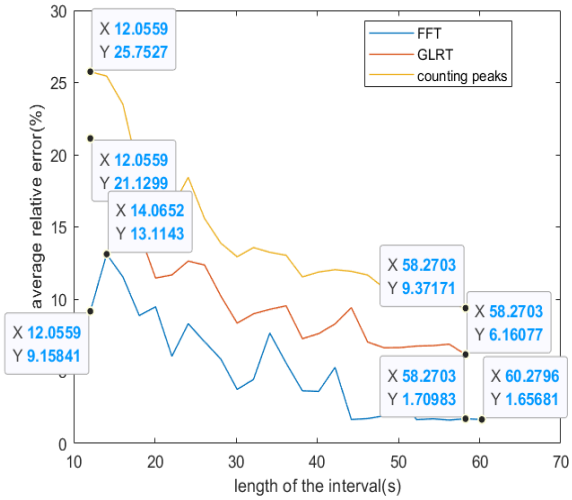

Figure 4.22: Average relative error of all people over different lengths of the intervals(constant ground truth heartbeat frequency pattern)

The simulation results of non-constant respiration frequency over different lengths of intervals are shown in Figure 4.23 and Figure 4.24. The GLRT method has a lower relative error of 12.55%-45.95% than the other two methods. The FFT method does not get higher accuracy when the intervals are longer because of the sidelobes caused by changing frequencies in the spectrum.

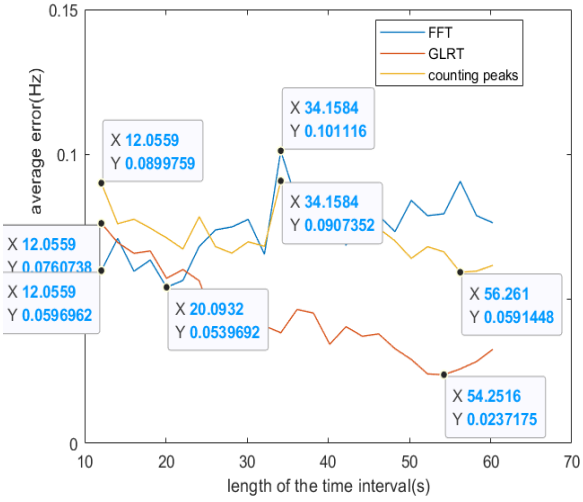

Figure 4.23: Average error of all people over different lengths of the intervals(non-constant ground truth heartbeat frequency pattern)

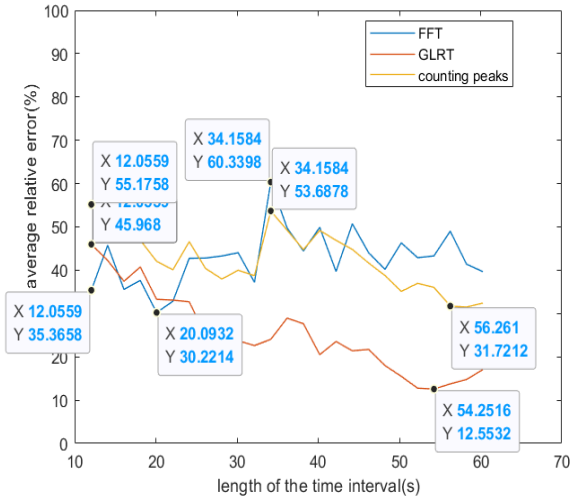

Figure 4.24: Average relative error of all people over different lengths of the intervals(non-constant ground truth heartbeat frequency pattern)

4.5. SUMMARY

The Monte Carlo strategy is used to evaluate the performance of the proposed pipeline with simulations as a function of different key factors, such as the length of the observation intervals. The results are summarized below. Three methods for the heartbeat estimation method are analyzed, including FFT, GLRT, and counting peaks.

- For constant heartbeat frequency, the FFT method has a lower relative error of all people than the other two methods, even with a relatively short interval of 2s. The error is limited by the interval length because of the Doppler resolution. The other two methods have a closely aligned margin of error because the ground truth frequency is stable with a perfect periodic heartbeat signal in the simulation.
- For non-constant heartbeat frequency, the FFT method has the lowest relative error with the length of the intervals as short as 2s. Because the interval length is short, the sidelobes of changing frequency do not influence the accuracy of the frequency peak selection in the spectrum. The GLRT method has a lower error than the counting peaks method after eliminating close peaks in the time domain caused by changing frequency.

The influence of the length of the observation intervals is analyzed in Section 4.2 and summarized below.

- When the length of the intervals is longer, the estimation accuracy is higher because of the higher Doppler resolution.
- For a constant heartbeat frequency, all three considered methods have higher accuracy with longer intervals. The FFT method has the lowest error of 4.88% with

intervals of 2 s and 0. 17% with intervals of 60 s shown in Figure 4.11. All three method can achieve a relative error lower than 1% when the length of the observation intervals is longer than 20 s.

- For non-constant heartbeat frequency, the FFT method has the lowest error when the length of the intervals is shorter than 4s. When the intervals are longer, the FFT method has a higher error than the other two methods because of the sidelobes from changing frequencies in the frequency domain. The GLRT method has the lowest error of 9.66% with intervals of 2s and 2.21% with intervals of 60 s shown in Figure 4.12.

The algorithm for RBM cancellation is evaluated by the confusion matrixes in Section 4.3.

- Two developed RBM models represent two kinds of large-scale movement that may occur in indoor healthcare when people are seated. They cannot simulate all possible RBM, but they can be simple and typical movement simulations like shaking the head and moving the chest.
- For both the constant and non-constant heartbeat frequency simulations, the detection algorithm has a good performance. The detection probability is between 89.5%-100%. The false alarm probability is between 1.6%-3.8%. The detection algorithm is effective.
- The intervals with detected RBM are discarded so that they do not influence the accuracy of the heartbeat estimation.

For completeness, beyond the heartbeat, the ability to estimate respiration is summarized below.

- For a constant respiration frequency, the accuracy is higher when the length of the interval increases from 12 to 60 s. The FFT method has a lower error between 1.66% with intervals of 14s and 13.11% with intervals of 60 s than the other two methods shown in Figure 4.22.
- For the non-constant respiration frequency, the GLRT method has a lower relative error of 45.95% with intervals of 12 s than the other two methods.

The analysis of the orientations and overlap percentages are shown in Appendix 7. The different orientations do not have a big effect on the results. The orientation is simply simulated by the radar cross section (RCS) of the chest with the plate, so it is not an optimal model. So, further analysis of the different orientations based on the experimental data is necessary. The different overlap percentages are also observed not to influence the estimation accuracy.

5

EXPERIMENTAL DATA COLLECTION AND RESULTS

The proposed processing pipeline is validated in this chapter with experimental data collected on purpose for this thesis. The experiment equipment and scenarios are introduced in Section 5.1. The new waveform used in experiments is designed in Section 5.2.1. The three estimation methods are discussed in Section 5.2.2. Section 5.2.3 and Section 5.2.6 analyze the influence of the length of the observation intervals and orientations. In Section 5.2.4 The results of the respiration frequency estimation are shown in 5.2.6

5.1. EXPERIMENTAL EQUIPMENT AND SCENARIO DESIGN

Seven test people are seated on a chair in front of the radar. The distance between the radar and the people is about 0.8m to give enough place for the radar, chair, and legs and provide higher signal-to-noise ratio (SNR) for the reflection signal from the chest. The test people sit in the same position but rotate the body in three directions: front side, left 30°and right 30°. The angle is the aspect angle to the line of sight (LoS) of the radar. The height of the radar is about the same height as the chest, the low height may detect the reflection from the abdomen, which may also have movements when breathing. The back of the test people is against the back of the chair to make the chest more stable because the heartbeat activity is weak. The information of the people measured on gender, height, BMI, age, and clothes are shown in Table 5.1. The measurement length is about 3 minutes to provide enough observation intervals. Figure 5.1 shows the scenario of the experiments with the front side.

Table 5.1: The information of the test people

	Gender	Age	Height(cm)	Weight(kg)	BMI(kg/m²)	Clothes
P1	Female	25	53	166	19.2	T-shirt
P2	Female	23	53	164	19.7	T-shirt
P3	Female	25	65	158	26	T-shirt
P4	Female	25	54	166	19.5	T-shirt
P5	Male	25	75	185	21.9	T-shirt
P6	Male	31	59	174	19.4	T-shirt
P7	Male	23	69	170	23.8	T-shirt

Figure 5.1: The scenario of the experiments with the front side facing the radar

The respiration belt is utilized to measure the ground truth respiration frequency [65]. The wrist oximeter is used to measure ground truth heartbeat frequency wrist oximeter CheckmeO2 Max [66]. The equipments are shown in Figure 5.2.

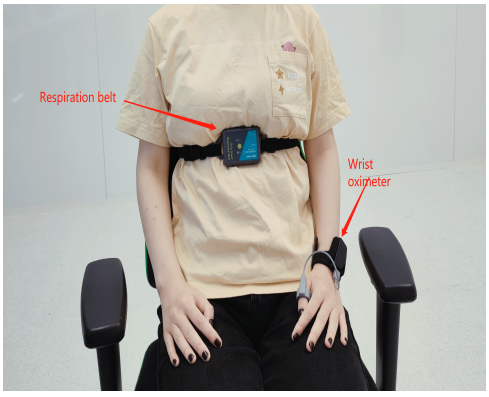

Figure 5.2: The respiration belt and wrist oximeter used as ground truth for the measurements

5.2. RESULTS AND ANALYSIS

5.2.1. DIFFERENT WAVEFORMS

The waveform used in the simulation has a chirp time of 5260us. The frequency band of the summed levels is 0.743-2.971 Hz, suitable for the heartbeat frequency of 1-3Hz. But in the experimental scenarios, the test people sit on a chair without doing any sports and have a heartbeat frequency typically lower than 2 Hz. The wrist oximeter will warn when the heartbeat frequency is higher than 2 Hz when sitting. At the beginning of the measurement test, it was found that one person sometimes had a low heartbeat frequency of approximately 0.88 Hz, shown in Figure 5.3 during measurement. When the frequency is close to the edge of the frequency band, the heartbeat signal is suppressed and the estimation error is higher. Therefore, the waveform is adjusted to fit the scenario of sitting and the lower heartbeat frequency. The design of the new waveform is shown in the third column of Table 3.1. The chirp time is set as 3900 us. Then, the new waveform can have a frequency band of 0.501-2.003 Hz, which includes the possible heartbeat frequency and makes the low frequency of 0.88 Hz far away from the edge of the frequency band and has higher accuracy.

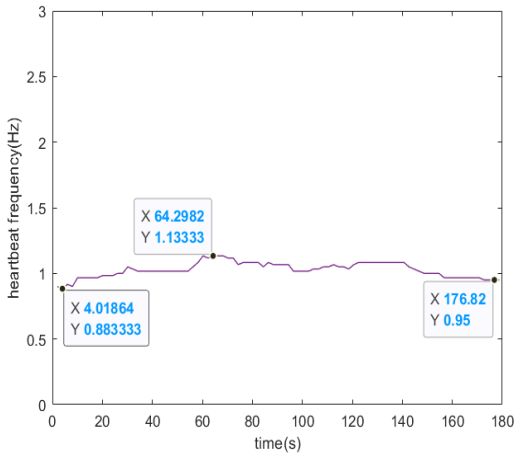

Figure 5.3: Ground truth heartbeat frequency measured by the wrist oximeter

5.2.2. HEARTBEAT FREQUENCY ESTIMATION METHODS

The error of different people with observation intervals of 2s by three estimation methods is shown in Figure 5.4. The results with observation intervals of 4s, 12s, and 40s are shown in Appendix 7. The error of different people is the average error of all the observation intervals for each people. It is observed that the method of counting peaks has the lowest error for most people. The FFT method has the highest error for all people.

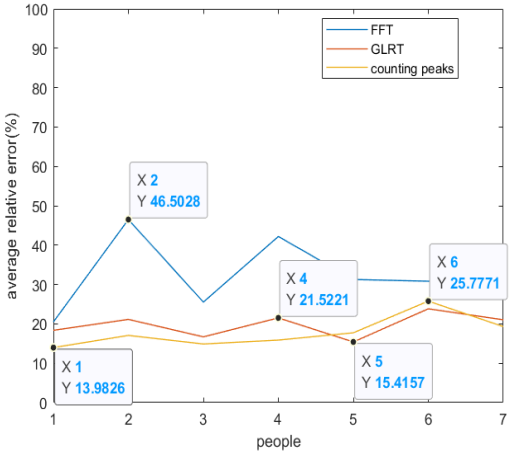

Figure 5.4: Average relative error for different people with observation intervals of 2s using three heartbeat estimation methods

In the simulations, the impulse-like artifacts caused by the unwrapping step is very small for the phase history difference. But in the experimental data, the impulse-like artifacts are very large, shown in Figure 5.5. The median filter can help reduce the impulse-like artifacts but can not remove the influence entirely and may smooth the weak heartbeat signal. The sidelobes caused by the noise in the frequency domain influence the selection of correct heartbeat peaks.

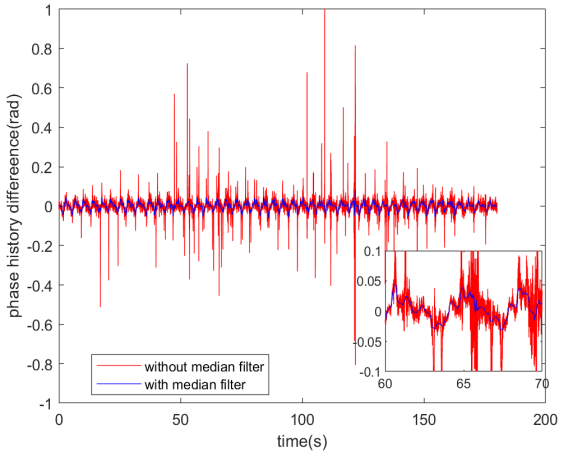

Figure 5.5: Phase history difference over time with and without applying a median filter(zoom-in figure between 60-70s in the lower right corner)

The GLRT method has a little higher error than the counting peaks method for most

test people. Because the distribution of heartbeat signal in experiments shown in Figure 5.6 does not fit very well with the normal distribution like simulations. It influences the precision of selecting a suitable amplitude threshold for counting heartbeat peaks.

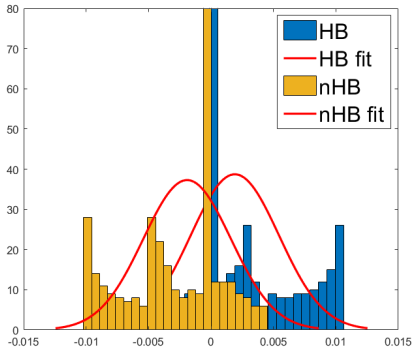

Figure 5.6: Histogram of HB and nHB values and fitted distributions of the experimental data(facing the radar with the front side and without RBM)

5.2.3. LENGTHS OF OBSERVATION INTERVALS

Figure 5.7 shows the average error over different lengths of observation intervals. When the length of observation intervals increases from 2s to 4s, the error decreases significantly for the three methods because the Doppler resolution increases from 0.5 Hz to 0.25 Hz. After increasing the interval higher than 4 s, the accuracy increases slower. Because the Doppler resolution is high enough, the selection of the estimation method is the critical factor determining the error. When the observation intervals are 34s, the FFT and GLRT methods achieve the lowest errors of 19.93% and 12.54%. The lowest error for the counting peaks methods is 8.14% with observation intervals of 44 s.

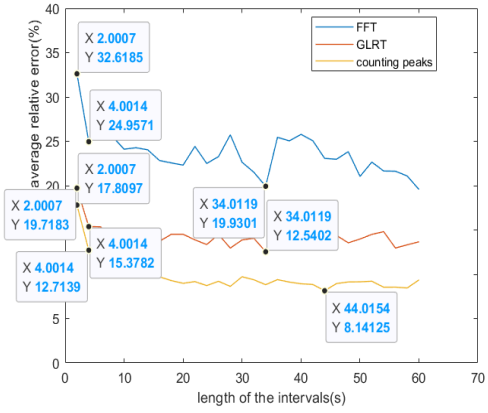

Figure 5.7: Average relative error of all people over different lengths of observation intervals

5.2.4. RANDOM BODY MOVEMENT CANCELLATION

There are two RBM models simulated in the simulations. It makes the RBM simple and determined. In experiments, RBM is random and larger than chest displacement due to the vital sign. The test people can move the chest in all directions, hands up, touch the head by hands, shake the head, and so on. The duration of the RBM is 15s which means the people can do multiple RBM. The left hand with the Wrist oximeter can not move to keep the high accuracy of the ground truth data.

The confusion matrix of RBM detection for all the people is shown in Figure 5.8. The performance of detection is good enough. The correct decision probability is 92.1%, meaning most of the RBM intervals are detected. The false alarm probability is 3.4%, indicating that not many observation intervals without RBM are wrongly detected.

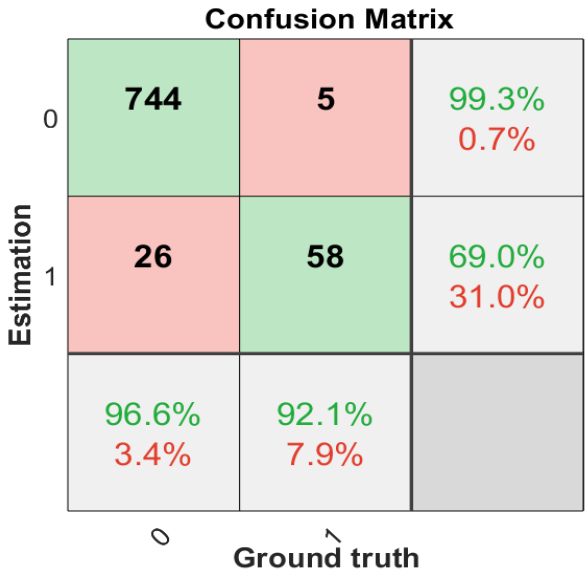

Figure 5.8: Confusion matrix of undetermined RBM detection of seven test people

5.2.5. ORIENTATION OF TARGETS

The average error of different orientations over different people is estimated by three methods shown in Appendix 7. The length of the observation intervals is 2s. The results are organized in Table 5.2. The front side has the lowest error of 22.38%. Because the orientations of the target influence the RCS, which is proportional to the received power of the signal. When people are facing the radar, the chest has the highest RCS. The higher SNR can increase the phase sensitivity for the heartbeat frequency estimation based on the phase history difference [48]. The counting peaks method has better performance in all orientations.

Table 5.2: Average relative error of all people of heartbeat estimation in different orientations

	FFT	GLRT	counting peaks	Average relative error of different methods(%)
Front	32.62	19.72	17.81	22.38
left 30 degrees	35.19	22.07	21.40	26.22
right 30 degrees	33.29	22.24	21.70	25.74
Average relative error of different orientations(%)	33.70	21.34	20.30	

5.2.6. RESPIRATION ESTIMATION

The average relative error over different lengths of observation intervals is shown in Figure 5.9. When the observation intervals are shorter than 30 s, the FFT method has the lowest error between 5.96% and 17.68%. When the length of the observation intervals increases higher than 40 s, the GLRT method has an error between 3.35% with intervals of 110 s and 9.25% with intervals of 40 s. The counting peaks method has an error between 16.03% with intervals of 100 s and 35.02% with intervals of 10 s. Overall, the GLRT method has higher accuracy in estimating respiration with longer observation intervals.

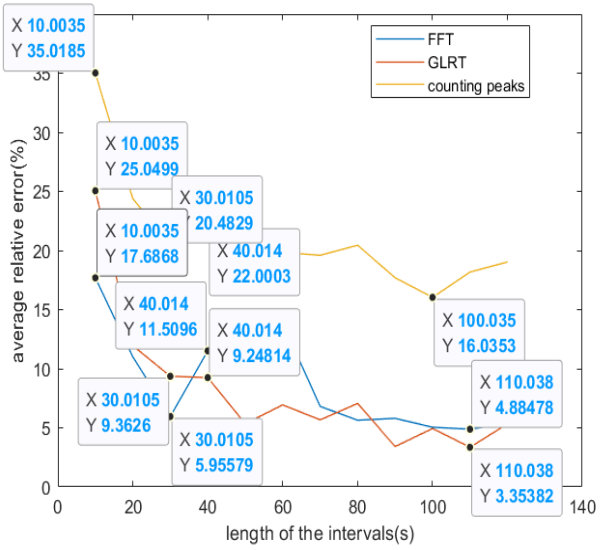

Figure 5.9: Average relative error of all people over different lengths of observation intervals(respiration)

The length of observation intervals is defined as 10s. The average error of all people over different orientations by three methods is shown in Appendix 7. The results are summarized in 5.3. The front side and left 30°have lower errors. The FFT method

performs better in all orientations, as shown in Figure 5.9.

Table 5.3: Average relative error of all people of respiration estimation in different orientations

	FFT	GLRT	counting peaks	Average relative error of different methods(%)
Front	17.69	25.05	35.02	25.92
left 30 degrees	15.61	23.16	36.94	25.24
right 30 degrees	32.04	25.43	37.49	31.66
Average relative error of different orientations(%)	21.78	24.55	36.48	

5.3. PERFORMANCE COMPARISON

The performance of the processing pipeline proposed in this project is compared to another representative paper using FMCW radars in Table 5.4. The algorithm using bandpass filter and FFT to estimate the frequency of vital signs [32] is applied to the same datasets without RBM measured by Waveform 2 in this thesis project.

Table 5.4: Estimation accuracy comparison to other paper

Method	WT and FFT	WT and GLRT	WT and counting peaks	Bandpass filter and FFT [32]
Radar	60GHz FMCW radar			80 GHz FMCW radar
Length of observation intervals(s)	2s-60s for heartbeat, 10s-120s for respiration			100s
Heartbeat error(%) (observation interval)	19.93(34s)-32.61(2s)	12.54(34s)-19.71(2s)	8.14(44s)-17.80(2s)	25.08
Respiration error(%) (observation interval)	4.88(110s)-17.69(10s)	3.35(110s)-25.05(10s)	16.04(100s)-35.01(10s)	15.88

The length of observation intervals is a crucial parameter for the estimation accuracy. The algorithm in the paper [32] uses the intervals of 100s. All three estimation methods proposed in this project can achieve a lower error with shorter intervals in estimating heartbeat frequency than the bandpass filter and FFT method. The FFT and GLRT methods also can achieve lower errors in estimating respiration frequency with shorter intervals. The proposed processing pipeline uses MODWT in this thesis project, which is robust to the noise and more accurate in separating the vital sign signal and noise compared with the bandpass filter and FFT method in the paper. The median filter also helps reduce the impulse-like artifacts caused by unwrapping. Furthermore, there are also other methods in the literature review that can be compared to the proposed

processing pipeline. However, due to the time limitation of this thesis project, it can be explored in future work.

5.4. SUMMARY

The proposed processing pipeline is validated by experimental radar data collected for the purpose of this thesis and involving seven participants. The main conclusions of this chapter are summarized below.

- The waveform defined in the third column of Table 3.1 is improved to fit the scenario of sitting people. It was found that the phase history difference suffered from the impulse-like artifacts caused by the unwrapping step. The median filter is added to reduce them.
- For the heartbeat estimation method, the FFT method has the highest error because there are still some impulse-like artifacts left in the phase history difference. The GLRT method has a slightly higher error than the counting peaks method because of the fitting distribution for most test people.
- For the length of the observation intervals, the higher resolution, the error for the three methods is lower because of the higher Doppler resolution. The test people have a stable heartbeat frequency during the measurement. The counting method has a lower error than the other two methods and can achieve a relative error of 8.14% with intervals of 44s and 17.81% with intervals of 2s.
- The influence of orientations of the front, left 30° and right 30° is discussed in Section 5.2.6. The front side has better performance because of the larger RCS. The counting peaks method has a lower error in three directions.
- For the results of the respiration estimation, the FFT method has the lowest error when the intervals are shorter than the 30s. The GLRT method has a higher accuracy when the interval is longer. The FFT method performs better in all orientations. The front side and left 30° have lower errors.
- The proposed processing pipeline is compared with the bandpass and FFT method with the same datasets measured by Waveform 2. The GLRT and FFT methods implemented in this thesis project have higher accuracy with shorter observation intervals in the heartbeat and respiration frequency estimation referred to Table 5.4.

6

CONCLUSIONS AND RECOMMENDATIONS

The conclusions of the whole thesis project are drawn in 6.1. The recommendations describe the limitations of this project in Section 6.2.

6.1. CONCLUSIONS

This thesis has designed a new waveform and a processing pipeline for heartbeat estimation and validated it with simulations and experiments. The main conclusions of the proposed processing pipeline, the simulation results, and the experiment results are drawn below.

- The heartbeat and respiration can be detected by the same radar waveform designed in Section 3.1.2 and Section 5.2.1. The phase history difference over the slow time is selected to extract the weak heartbeat signal. The wavelet transform algorithm can be applied for heartbeat and respiration estimation with multi-resolution analysis.
- Three estimation methods, including FFT, GLRT, and counting peaks, are discussed to calculate the heartbeat frequency in frequency and time domains. Monte Carlo simulation and experimental data are used to evaluate the performance of the algorithm.
- In simulations, it was found that the FFT method is suitable for the constant heartbeat frequency. This can achieve 4.88% with short observation intervals of 2s and 0.17% with observation intervals of 60s referred to Figure 4.11. The FFT method is not robust to the non-constant heartbeat frequency because of the sidelobes caused by changing frequency in the frequency domain. It has a higher error of 6.71% with intervals of 6s and 23.11% with intervals of 36s referred to Figure 4.12. The counting peaks and GLRT methods perform well for constant and non-constant heartbeat frequencies. The GLRT method has higher accuracy for the

non-constant frequency because of two thresholds to select heartbeat peaks and can achieve 9.66% with intervals of 2s and 2.21% with intervals of 56s shown in Figure 4.12. The counting peaks method has a relative error of 10.99% with intervals of 2s and 3.98% with intervals of 60s for non-constant heartbeat frequency shown in Figure 4.12.

- In experiments, seven test people were seated and measured. The counting peaks method has better performance than the other two methods in heartbeat frequency estimation with intervals of 2 s shown in Figure 5.7. Although the heartbeat frequency is stable during measurements, it was found that the impulse-like artifacts were caused by unwrapping, the median filter was added to try and smoothen them out. However, the signal is not as clean as the simulation. Then, the FFT method is affected by this and has lower accuracy. The GLRT method has a higher error because the distribution of the heartbeat and no heartbeat points does not fit very well with the normal distribution like simulations.

- The length of the intervals is the crucial parameter to determine the estimation accuracy for heartbeat and respiration frequency estimation. When the length of observation intervals is longer, the Doppler resolution to detect the vital signs signal is higher. The counting peaks method can get a lower relative error than the other two methods and can achieve a relative error of 8.14% with intervals of 44s and 17.80% with intervals of 2s in heartbeat frequency estimation in experiments referred to Figure 5.7. For respiration frequency estimation, the GLRT method can achieve the lowest error of 3.35% with observation intervals of 110s shown in Figure 5.9. For shorter intervals of 30 s, the FFT method has a lower relative error of 5.96%.

- The energy threshold of phase history difference is used to detect the random body movement. Two simple models of large-scale movement are simulated, and the algorithm works well. More undetermined random movements like shaking hands, touching the head, and moving the chest in random directions are tested in the experiments. The detection algorithm is effective and can achieve a correct decision probability of 92.1% in experiments shown in Figure 5.8. The false alarm probability is 3.4%.

- The different orientations are simulated by different RCS of a plate, which is not an optimal simulation model. There is no big difference between different orientations in simulations. The orientations of the front side left 30°, and right 30°are tested in experiments. The front side is found to have a higher heartbeat and respiration frequency estimation accuracy because of the larger RCS of the chest reflection to the radar.

- The proposed processing pipeline is compared with the bandpass and FFT method with the same datasets. The GLRT and FFT methods implemented in this thesis project have higher accuracy with shorter observation intervals in the heartbeat and respiration frequency estimation referred to Table 5.4.

6.2. RECOMMENDATIONS

The recommendations of this project are described below.

- The group of test people is not too large, more test people with various ages and clothes can support a thorough validation of the robustness of the algorithm.
- The people are seated in this project, and more scenarios like standing, moving, and so on can be tested and studied. The range between the people tested and the radar is fixed, and the influence of the range can be tested and discussed. The orientation selection of this project is limited by time, more orientations like left, right, and back sides can be tested.
- The large-scale random body movement is detected and discarded in this project. There are also some RBM with a small scale that can be studied and canceled. The algorithm in this thesis project discarded the observation intervals with RBM. If there are too many RBM in some scenarios such as walking, the effectiveness of capturing the heartbeat frequency is low. The approaches to recover the data with RBM like [27] and estimate the vital sign frequency can be explored.
- This thesis project utilized the FMCW radar to measure vital signs. Other radars such as the impulse radio ultra-wideband (IR-UWB) radar [38], are also applied to extract vital signs in other papers with high accuracy. The algorithm can also be applied to the data measured by IR-UWB radars and compare the performance with the FMCW radar.

BIBLIOGRAPHY

[1] Max CORTES PERALTA. "Joint human motion recognition and breathing frequency estimation for indoor healthcare applications". 2022.

[2] US Department of Health, Human Services, et al. *The National Alliance for Health Information Technology report to the Office of the National Coordinator for Health Information Technology on defining key health information technology terms*. 2008.

[3] Alan R Dyer et al. "Heart rate as a prognostic factor for coronary heart disease and mortality: findings in three Chicago epidemiologic studies". In: *American journal of epidemiology* 112.6 (1980), pp. 736–749.

[4] David Nanchen. "Resting heart rate: what is normal?" In: *Heart* 104.13 (2018), pp. 1048–1049. ISSN: 1355-6037. DOI: 10.1136/heartjnl-2017-312731. eprint: https://heart.bmj.com/content/104/13/1048.full.pdf. URL: https://heart.bmj.com/content/104/13/1048.

[5] Dongfeng Zhang, Weijing Wang, and Fang Li. "Association between resting heart rate and coronary artery disease, stroke, sudden death and noncardiovascular diseases: a meta-analysis". In: *Cmaj* 188.15 (2016), E384–E392.

[6] Fabio Weishaupt et al. "Vital Sign Localization and Measurement Using an LFMCW MIMO Radar". In: *2018 19th International Radar Symposium (IRS)*. 2018, pp. 1–8. DOI: 10.23919/IRS.2018.8448229.

[7] Alessandra Galli et al. "An Overview of the Sensors for Heart Rate Monitoring Used in Extramural Applications". In: *Sensors* 22.11 (2022). ISSN: 1424-8220. DOI: 10.3390/s22114035. URL: https://www.mdpi.com/1424-8220/22/11/4035.

[8] P Marchionni et al. "An optical measurement method for the simultaneous assessment of respiration and heart rates in preterm infants". In: *Review of Scientific Instruments* 84.12 (2013).

[9] Nathan Jeger-Madiot et al. "Non-contact and through-clothing measurement of the heart rate using ultrasound vibrocardiography". In: *Medical Engineering Physics* 50 (2017), pp. 96–102. ISSN: 1350-4533. DOI: https://doi.org/10.1016/j.medengphy.2017.09.003. URL: https://www.sciencedirect.com/science/article/pii/S1350453317302552.

[10] Qian Xu et al. "Emotion monitoring with RFID: an experimental study". In: *CCF Transactions on Pervasive Computing and Interaction* 2.4 (2020), pp. 299–313.

[11] Noah Hafner et al. "Non-Contact Cardiopulmonary Sensing with a Baby Monitor". In: *2007 29th Annual International Conference of the IEEE Engineering in Medicine and Biology Society*. 2007, pp. 2300–2302. DOI: 10.1109/IEMBS.2007.4352785.

[12] Giulia Sacco et al. “An FMCW Radar for Localization and Vital Signs Measurement for Different Chest Orientations”. In: *Sensors* 20.12 (2020). ISSN: 1424-8220. DOI: 10.3390/s20123489. URL: https://www.mdpi.com/1424-8220/20/12/3489.

[13] Mehrdad Nosrati and Negar Tavassolian. “Accuracy Enhancement of Doppler Radar-Based Heartbeat Rate Detection Using Chest-Wall Acceleration”. In: *2018 IEEE International Microwave Biomedical Conference (IMBioC)*. 2018, pp. 139–141. DOI: 10.1109/IMBIOC.2018.8428898.

[14] John E Hall and Michael E Hall. *Guyton and Hall textbook of medical physiology e-Book*. Elsevier Health Sciences, 2020.

[15] AE Aubert et al. “Laser method for recording displacement of the heart and chest wall”. In: *Journal of biomedical engineering* 6.2 (1984), pp. 134–140.

[16] Kimio Konno and Jere Mead. “Measurement of the separate volume changes of rib cage and abdomen during breathing”. In: *Journal of applied physiology* 22.3 (1967), pp. 407–422.

[17] Faranak Mohammad-Zadeh, Farhad Taghibakhsh, and Bozena Kaminska. “Contactless heart monitoring (CHM)”. In: *2007 Canadian Conference on Electrical and Computer Engineering*. IEEE. 2007, pp. 583–585.

[18] Marco Baldi et al. “Body movement compensation in UWB radars for respiration monitoring”. In: *2012 IEEE First AESS European Conference on Satellite Telecommunications (ESTEL)*. 2012, pp. 1–6. DOI: 10.1109/ESTEL.2012.6400084.

[19] Giacomo Paterniani et al. “Radar-Based Monitoring of Vital Signs: A Tutorial Overview”. In: *Proceedings of the IEEE* 111.3 (2023), pp. 277–317. DOI: 10.1109/JPROC.2023.3244362.

[20] Antonio Lazaro, David Girbau, and Ramon Villarino. “Techniques for Clutter Suppression in the Presence of Body Movements during the Detection of Respiratory Activity through UWB Radars”. In: *Sensors* 14.2 (2014), pp. 2595–2618. ISSN: 1424-8220. DOI: 10.3390/s140202595. URL: https://www.mdpi.com/1424-8220/14/2/2595.

[21] Rudolf Zetik, Snezhana Jovanoska, and Reiner Thomä. “Simple method for localisation of multiple tag-free targets using UWB sensor network”. In: *2011 IEEE International Conference on Ultra-Wideband (ICUWB)*. 2011, pp. 268–272. DOI: 10.1109/ICUWB.2011.6058843.

[22] G. Sacco et al. “Vital Signs Monitoring for Different Chest Orientations Using an FMCW Radar”. In: *2020 XXXIIIrd General Assembly and Scientific Symposium of the International Union of Radio Science*. 2020, pp. 1–4. DOI: 10.23919/URSIGASS49373.2020.9232333.

[23] Sukhvinder Singh et al. “Sense through wall human detection using UWB radar”. In: *EURASIP Journal on Wireless Communications and Networking* 2011.1 (2011), pp. 1–11.

[24] Daehyeon Yim and Sung Ho Cho. “An equidistance multi-human detection algorithm based on noise level using mono-static IR-UWB radar system”. In: (Feb. 2015), pp. 131–134. DOI: 10.1201/b18049-31.

[25] Faheem Khan and Sung Ho Cho. “A detailed algorithm for vital sign monitoring of a stationary/non-stationary human through IR-UWB radar”. In: *Sensors* 17.2 (2017), p. 290.

[26] Min Xu et al. “An adaptive Kalman filter technique for context-aware heart rate monitoring”. In: *2012 Annual International Conference of the IEEE Engineering in Medicine and Biology Society*. 2012, pp. 6522–6525. DOI: 10.1109/EMBC.2012.6347488.

[27] Changzhi Li and Jenshan Lin. “Complex signal demodulation and random body movement cancellation techniques for non-contact vital sign detection”. In: *2008 IEEE MTT-S International Microwave Symposium Digest*. IEEE. 2008, pp. 567–570.

[28] Changzhan Gu et al. “Doppler radar vital sign detection with random body movement cancellation based on adaptive phase compensation”. In: *2013 IEEE MTT-S International Microwave Symposium Digest (MTT)*. 2013, pp. 1–3. DOI: 10.1109/MWSYM.2013.6697618.

[29] Qinyi Lv et al. “Detection of bio-signals from body movement based on high-dynamic-range Doppler radar sensor”. In: *2015 IEEE MTT-S 2015 International Microwave Workshop Series on RF and Wireless Technologies for Biomedical and Healthcare Applications (IMWS-BIO)*. IEEE. 2015, pp. 88–89.

[30] José-María Muñoz-Ferreras et al. “Random body movement mitigation for FMCW-radar-based vital-sign monitoring”. In: *2016 IEEE Topical Conference on Biomedical Wireless Technologies, Networks, and Sensing Systems (BioWireleSS)*. 2016, pp. 22–24. DOI: 10.1109/BIOWIRELESS.2016.7445551.

[31] Tjahjo Adiprabowo et al. “Human Vital Signs Detection: A Concurrent Detection Approach”. In: *Applied Sciences* 12.3 (2022). ISSN: 2076-3417. URL: https://www.mdpi.com/2076-3417/12/3/1077.

[32] Siying Wang et al. “A novel ultra-wideband 80 GHz FMCW radar system for contactless monitoring of vital signs”. In: *2015 37th Annual International Conference of the IEEE Engineering in Medicine and Biology Society (EMBC)*. 2015, pp. 4978–4981. DOI: 10.1109/EMBC.2015.7319509.

[33] Wei Ren et al. “Vital Sign Detection in Any Orientation Using a Distributed Radar Network via Modified Independent Component Analysis”. In: *IEEE Transactions on Microwave Theory and Techniques* 69.11 (2021), pp. 4774–4790. DOI: 10.1109/TMTT.2021.3101655.

[34] Giulia Sacco et al. “An FMCW radar for localization and vital signs measurement for different chest orientations”. In: *Sensors* 20.12 (2020), p. 3489.

[35] Lingyun Ren et al. “Investigation of vital signs monitoring errors due to subject’s orientation, clothing and distance from a SFCW radar”. In: *2016 IEEE International Symposium on Antennas and Propagation (APSURSI)*. 2016, pp. 1171–1172. DOI: 10.1109/APS.2016.7696293.

[36] Srikrishna Iyer et al. “mm-Wave radar-based vital signs monitoring and arrhythmia detection using machine learning”. In: *Sensors* 22.9 (2022), p. 3106.

[37] Sabikun Nahar et al. “An Electromagnetic Model of Human Vital Signs Detection and Its Experimental Validation”. In: *IEEE Journal on Emerging and Selected Topics in Circuits and Systems* 8.2 (2018), pp. 338–349. DOI: 10.1109/JETCAS.2018.2811339.

[38] Antonio Lazaro, David Girbau, and Ramon Villarino. “Analysis of vital signs monitoring using an IR-UWB radar”. In: *Progress In Electromagnetics Research* 100 (2010), pp. 265–284.

[39] Lawrence R. Rabiner, Ronald W. Schafer, and Charles M. Rader. “The chirp z-transform algorithm and its application”. In: *The Bell System Technical Journal* 48.5 (1969), pp. 1249–1292. DOI: 10.1002/j.1538-7305.1969.tb04268.x.

[40] Marco Mercuri et al. “A Direct Phase-Tracking Doppler Radar Using Wavelet Independent Component Analysis for Non-Contact Respiratory and Heart Rate Monitoring”. In: *IEEE Transactions on Biomedical Circuits and Systems* 12.3 (2018), pp. 632–643. DOI: 10.1109/TBCAS.2018.2813013.

[41] Norden E. Huang et al. “The empirical mode decomposition and the Hilbert spectrum for nonlinear and non-stationary time series analysis”. In: *Proceedings of the Royal Society of London. Series A: Mathematical, Physical and Engineering Sciences* 454 (1998), pp. 903–995.

[42] Zhaohua Wu and Norden E Huang. “Ensemble empirical mode decomposition: a noise-assisted data analysis method”. In: *Advances in adaptive data analysis* 1.01 (2009), pp. 1–41.

[43] Konstantin Dragomiretskiy and Dominique Zosso. “Variational Mode Decomposition”. In: *IEEE Transactions on Signal Processing* 62.3 (2014), pp. 531–544. DOI: 10.1109/TSP.2013.2288675.

[44] Kuan Ju Wu and Chin-Lung Yang. “Heart Rate Extraction with VMD Algorithm in Non-Stationary Clutter Environment Based on FMCW Radar Systems”. In: *2021 IEEE International Symposium on Radio-Frequency Integration Technology (RFIT)*. 2021, pp. 1–3. DOI: 10.1109/RFIT52905.2021.9565243.

[45] Ilya V Mikhelson et al. “Remote sensing of patterns of cardiac activity on an ambulatory subject using millimeter-wave interferometry and statistical methods”. In: *Medical & biological engineering & computing* 51.1 (2013), pp. 135–142.

[46] Olivier Rioul and Martin Vetterli. “Wavelets and signal processing”. In: *IEEE signal processing magazine* 8.4 (1991), pp. 14–38.

[47] A. Tariq and H. G. Shiraz. “Doppler radar vital signs monitoring using wavelet transform”. In: *2010 Loughborough Antennas Propagation Conference*. 2010, pp. 293–296. DOI: 10.1109/LAPC.2010.5666002.

[48] Adeel Ahmad et al. “Vital signs monitoring of multiple people using a FMCW millimeter-wave sensor”. In: *2018 IEEE Radar Conference (RadarConf18)*. 2018, pp. 1450–1455. DOI: 10.1109/RADAR.2018.8378778.

[49] Nicusor Birsan et al. “Time-frequency analysis in Doppler radar for noncontact cardiopulmonary monitoring”. In: *2011 E-Health and Bioengineering Conference (EHB)*. 2011, pp. 1–4.

[50] A.D. Droitcour et al. “Range correlation and I/Q performance benefits in single-chip silicon Doppler radars for noncontact cardiopulmonary monitoring”. In: *IEEE Transactions on Microwave Theory and Techniques* 52.3 (2004), pp. 838–848. DOI: 10.1109/TMTT.2004.823552.

[51] Changzhi Li et al. “Accurate Doppler Radar Noncontact Vital Sign Detection Using the RELAX Algorithm”. In: *IEEE Transactions on Instrumentation and Measurement* 59.3 (2010), pp. 687–695. DOI: 10.1109/TIM.2009.2025986.

[52] Hyunjae Lee et al. “A novel vital-sign sensing algorithm for multiple subjects based on 24-GHz FMCW Doppler radar”. In: *Remote Sensing* 11.10 (2019), p. 1237.

[53] Mohammad Shaifur Rahman, Byung-Jun Jang, and Ki-Doo Kim. “A new digital signal processor for Doppler radar cardiopulmonary monitoring system”. In: *2008 International Conference on Electrical and Computer Engineering*. 2008, pp. 76–79. DOI: 10.1109/ICECE.2008.4769176.

[54] Rudolph Emil Kalman. “A new approach to linear filtering and prediction problems”. In: (1960).

[55] Mohammad Shaifur Rahman et al. “Extended Kalman Filter for Doppler radar cardiopulmonary monitoring system”. In: *2012 7th International Conference on Electrical and Computer Engineering*. 2012, pp. 264–267. DOI: 10.1109/ICECE.2012.6471536.

[56] Muhammad Arsalan, Avik Santra, and Christoph Will. “Improved Contactless Heartbeat Estimation in FMCW Radar via Kalman Filter Tracking”. In: *IEEE Sensors Letters* 4.5 (2020), pp. 1–4. DOI: 10.1109/LSENS.2020.2983706.

[57] Laura Anitori, Ardjan de Jong, and Frans Nennie. “FMCW radar for life-sign detection”. In: *2009 IEEE Radar Conference*. 2009, pp. 1–6. DOI: 10.1109/RADAR.2009.4976934.

[58] P. Flandrin, G. Rilling, and P. Goncalves. “Empirical mode decomposition as a filter bank”. In: *IEEE Signal Processing Letters* 11.2 (2004), pp. 112–114. DOI: 10.1109/LSP.2003.821662.

[59] Changzhan Gu et al. “A Hybrid Radar-Camera Sensing System With Phase Compensation for Random Body Movement Cancellation in Doppler Vital Sign Detection”. In: *IEEE Transactions on Microwave Theory and Techniques* 61.12 (2013), pp. 4678–4688. DOI: 10.1109/TMTT.2013.2288226.

[60] Texas Instruments. *IWR6843, Single-chip 60-GHz to 64-GHz intelligent mmWave sensor integrating processing capability*. https://www.ti.com/product/IWR6843, Last accessed on 2023-5-30. 2020.

[61] Muhammad Najam Dar et al. “ECG biometric identification for general population using multiresolution analysis of DWT based features”. In: *2015 Second International Conference on Information Security and Cyber Forensics (InfoSec)*. 2015, pp. 5–10. DOI: 10.1109/InfoSec.2015.7435498.

[62] Donald B Percival and Andrew T Walden. *Wavelet methods for time series analysis*. Vol. 4. Cambridge university press, 2000.

[63] Youngmin Seo, Yunyoung Choi, and Jeongwoo Choi. “River Stage Modeling by Combining Maximal Overlap Discrete Wavelet Transform, Support Vector Machines and Genetic Algorithm”. In: *Water* 9.7 (2017). ISSN: 2073-4441. DOI: 10.3390/w9070525. URL: https://www.mdpi.com/2073-4441/9/7/525.

[64] Li Zhu, Yanxin Wang, and Qibin Fan. “MODWT-ARMA model for time series prediction”. In: *Applied Mathematical Modelling* 38.5 (2014), pp. 1859–1865. ISSN: 0307-904X. DOI: https://doi.org/10.1016/j.apm.2013.10.002. URL: https://www.sciencedirect.com/science/article/pii/S0307904X13006148.

[65] *Go Direct Respiration Belt*. https://www.vernier.com/product/go-direct-respiration-belt/. Accessed: 2022-12-09.

[66] *Wrist Oximeter Checkme O2 Max*. https://www.viatomtech.com/checkmeo2-max/. Accessed: 2022-12-09.

7

APPENDICES

APPENDIX A

The ten patterns of non-constant heartbeat frequency in simulations are shown in the figures below. The patterns have rising and falling or mutating heartbeats during the simulation time, to mimic different people or scenarios.

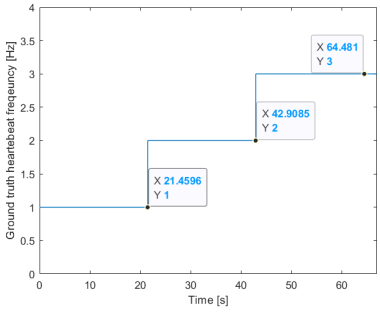

Figure 7.1: Non-constant heartbeat frequency (pattern 1)

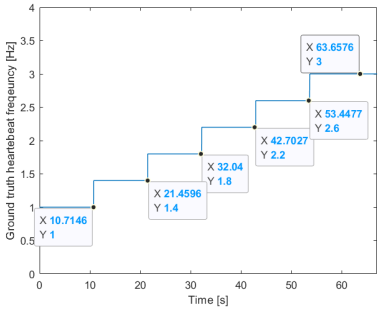

Figure 7.2: Non-constant heartbeat frequency (pattern 2)

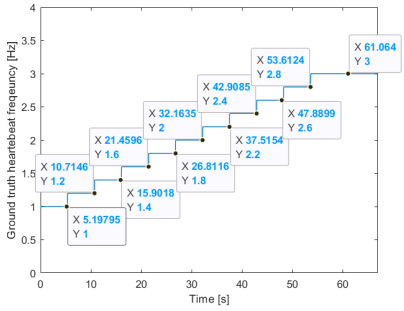

Figure 7.3: Non-constant heartbeat frequency (pattern 3)

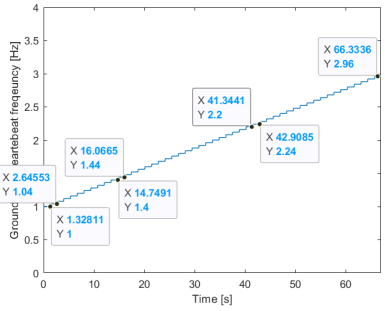

Figure 7.4: Non-constant heartbeat frequency (pattern 4)

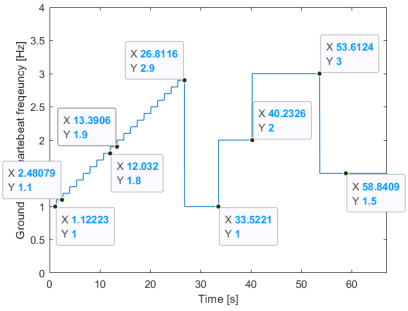

Figure 7.5: Non-constant heartbeat frequency (pattern 5)

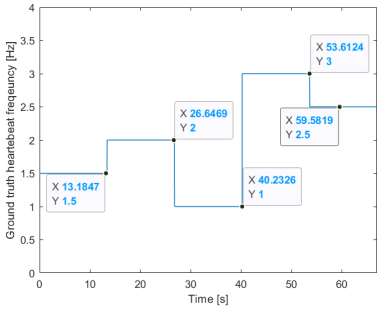

Figure 7.6: Non-constant heartbeat frequency (pattern 6)

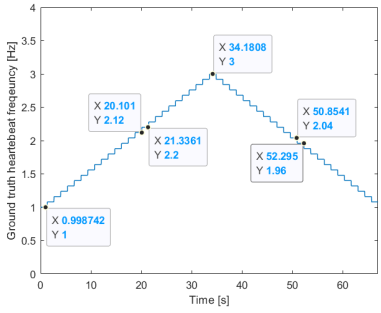

Figure 7.7: Non-constant heartbeat frequency (pattern 7)

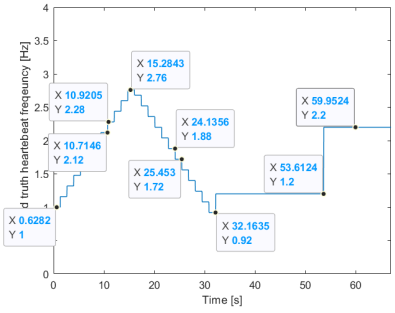

Figure 7.8: Non-constant heartbeat frequency (pattern 8)

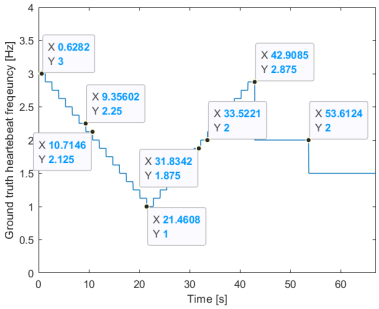

Figure 7.9: Non-constant heartbeat frequency (pattern 9)

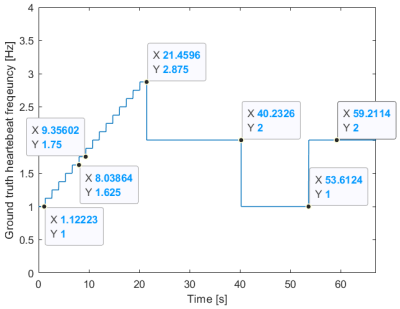

Figure 7.10: Non-constant heartbeat frequency (pattern 10)

APPENDIX B

OVERLAP OF INTERVALS

The influence of the overlap percentage on the estimation accuracy is also in simulations. The average relative error over different overlap percentages of constant simulations is shown in Figure 7.11. The length of the intervals is 12s. When the percentage of overlap between sequential intervals increases, the errors of the three methods do not change above 0.1%. The overlap does not provide more information for the constant heartbeat frequency estimation.

The average relative error over different overlap percentages of non-constant simulations is shown in Figure 7.12. The FFT method has the highest error of 9.74% because the length of observation intervals of 12 s is long for changing frequency. The GLRT method has the lowest error of 4.26% with observation intervals of 50 s. When the overlap percentage increases, the difference between the minimum and maximum error is not higher than 2.56% for the three methods. So the overlap can not improve the estimation accuracy when the ground truth heartbeat frequency changes over time.

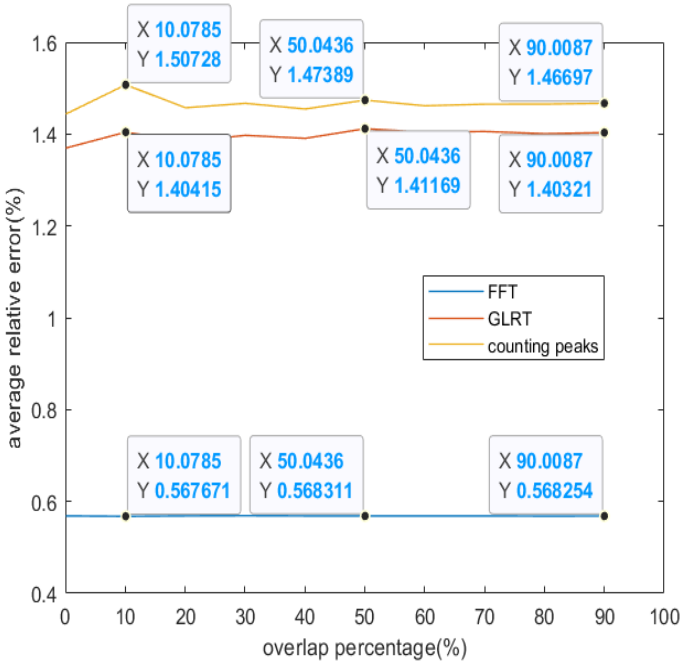

Figure 7.11: Average relative error of all people over different overlap percentage(constant ground truth heartbeat frequency pattern)

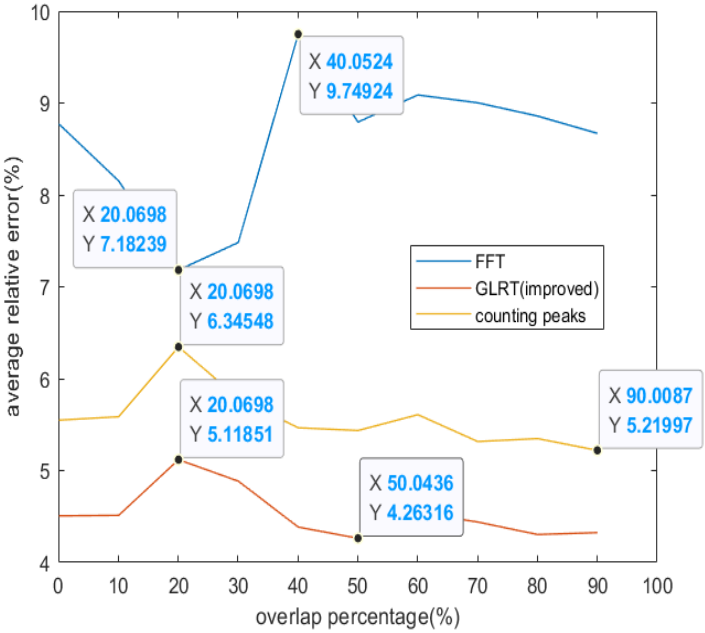

Figure 7.12: Average relative error of all people over different overlap percentage(non-constant ground truth heartbeat frequency pattern)

ORIENTATION OF TARGETS

The orientation of the targets changes the RCS (Radar Cross Section) which measures the power reflected to the radar and is proportional to the received power. It depends on the ratio of the physical size and the wavelength. If considering the RCS of the chest as a flat plate, the RCS of the chest is derived by Equation 7.1.

$$\sigma = \frac{4\pi a^2 b^2}{\lambda^2} \tag{7.1}$$

Here, a and b are the height and width of the plate, and λ is the wavelength of the radar which is determined by the frequency.

If the RCS of the front side is defined as the reference RCS which equals 1. Then the RCS of the target with different angles can be defined as $(\cos(\theta))^2$ based on Equation 7.1. θ is the angle between the line of sight of the radar and the target's front side, which is (0°,90°). The average error over different angles of constant frequency simulation is shown in Figure 7.13. The average error over different angles of non-constant frequency simulation is shown in Figure 7.14. The distribution of error over different orientations is irregular.

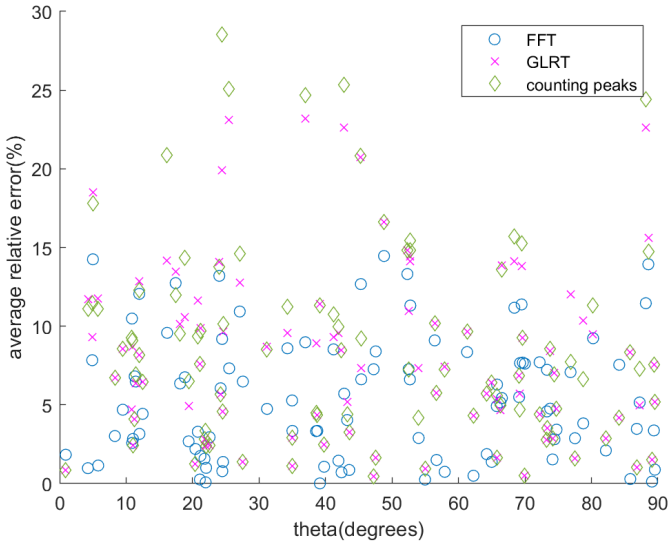

Figure 7.13: Average relative error over different angles(constant ground truth heartbeat frequency pattern)

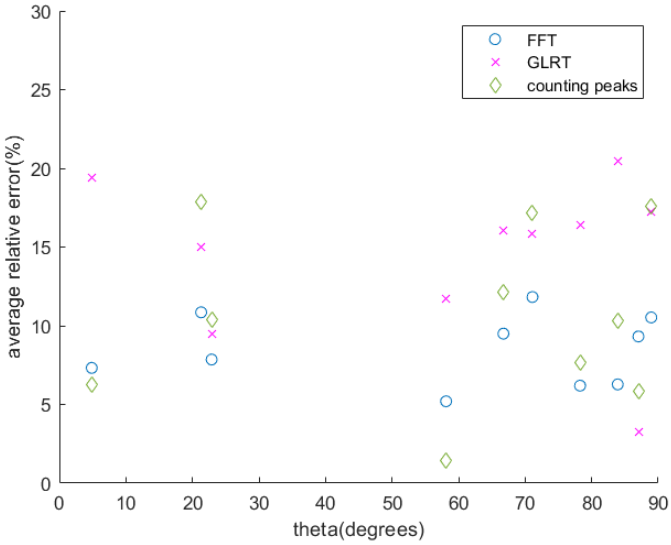

Figure 7.14: Average relative error over different angles(non-constant ground truth heartbeat frequency pattern)

APPENDIX C

The experimental results with observation intervals of 4s,12s, and 40s of different people are shown below.

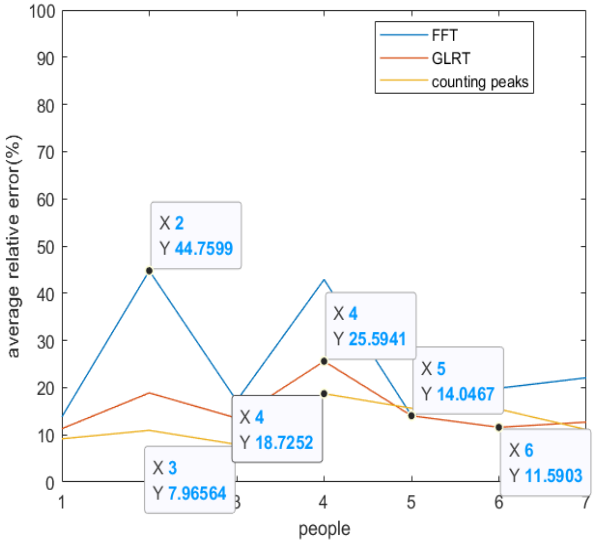

Figure 7.15: Average relative error of different people with intervals of 4s using three estimation methods

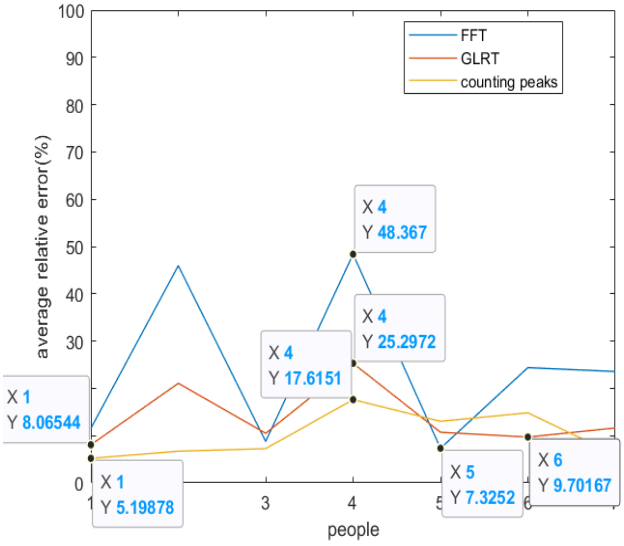

Figure 7.16: Average relative error of different people with intervals of 12s using three estimation methods

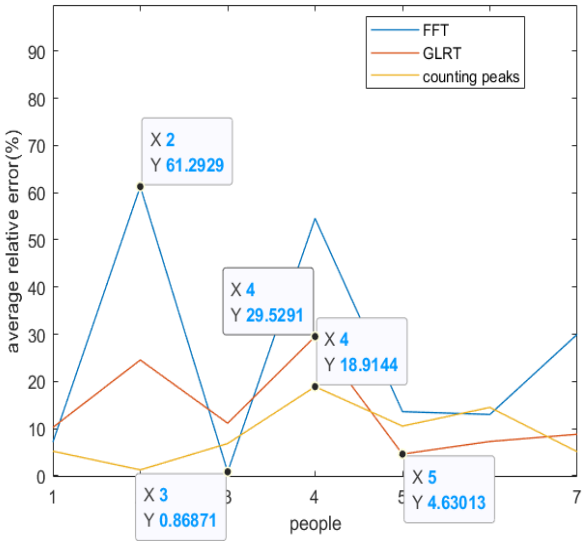

Figure 7.17: Average relative error of different people with intervals of 40s using three estimation methods

APPENDIX D

The average error over different overlap percentages of the experiments is shown in Figure 7.18. The length of intervals is 12s. The conclusion of the results is similar to the simulation of the constant heartbeat frequency. The change of average relative error is small than 2% when the overlap percentage changes.

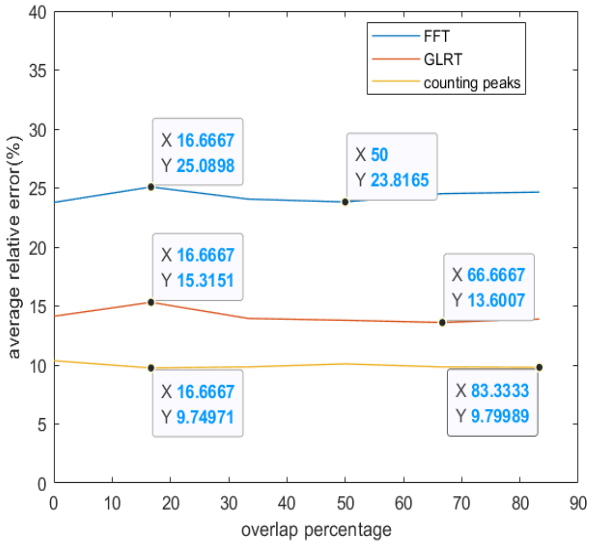

Figure 7.18: Average error of all people over different overlap percentage using three estimation methods

APPENDIX E

In this project, there are three different orientations: front side, left 30 degrees, and right 30 degrees in experiments. The average error with different orientations of different people is estimated by three methods shown below. The length of the observation intervals is 2 s.

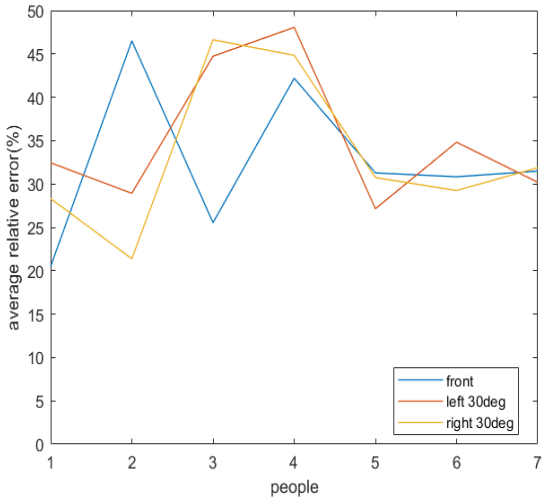

Figure 7.19: Average relative error of different people over different orientations(FFT method)

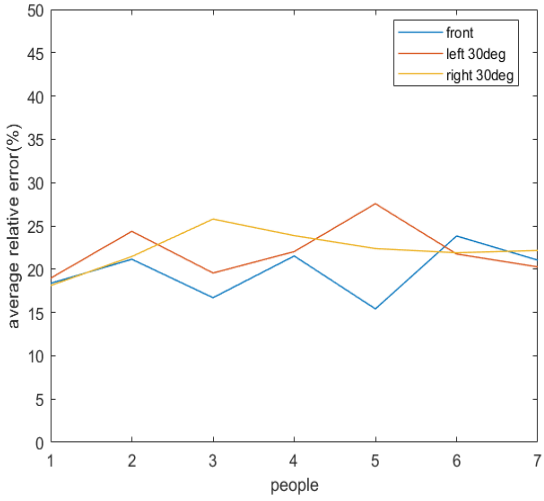

Figure 7.20: Average relative error of different people over different orientations(GLRT method)

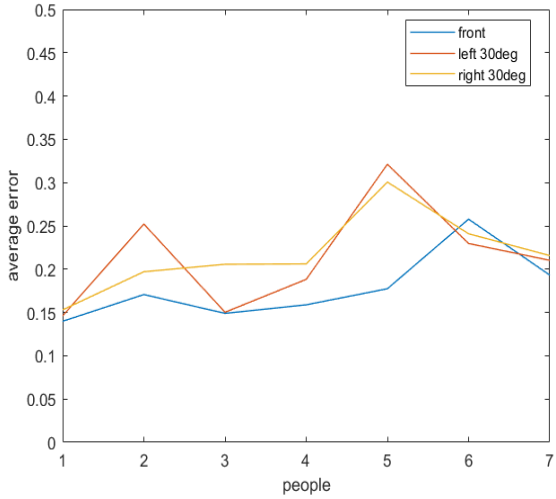

Figure 7.21: Average relative error of different people over different orientations(counting peaks method)

APPENDIX F

The length of the interval is defined as 10s. The average error of all people with different orientations by three methods is shown below.

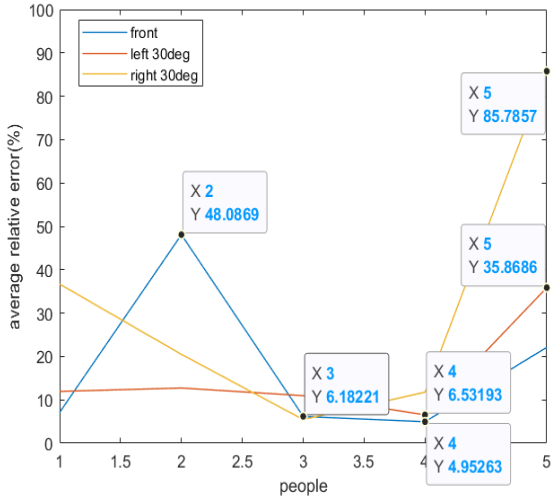

Figure 7.22: Average relative error of different people with different orientations(respiration,FFT method)

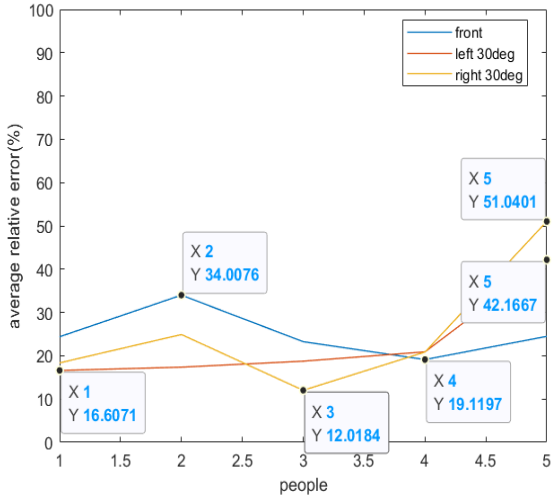

Figure 7.23: Average relative error of different people with different orientations(respiration,GLRT method)

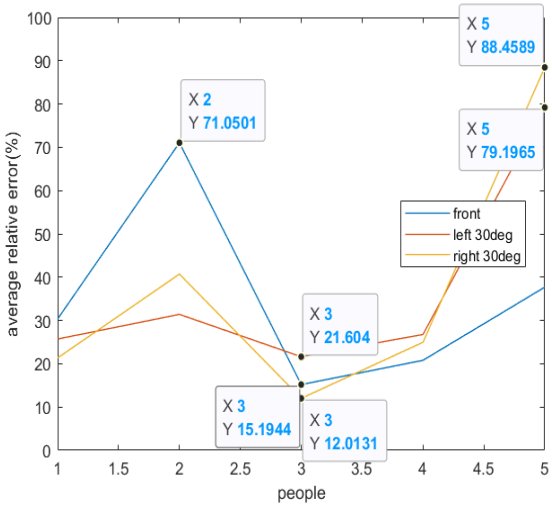

Figure 7.24: Average relative error of different people with different orientations(respiration,counting peaks method)